GEOLOGICA CARPATHICA, JUNE 2017, 68, 3, 229–247 doi: 10.1515/geoca-2017-0017

Geochemical and isotopic evidence for Carboniferous rifting: mafic dykes in the central Sanandaj-Sirjan zone (Dorud-Azna, West Iran)

FARZANEH SHAKERARDAKANI[1]✉, FRANZ NEUBAUER[1], MANFRED BERNROIDER[1], ALBRECHT VON QUADT[2], IRENA PEYTCHEVA[2], XIAOMING LIU[3], JOHANN GENSER[1], BEHZAD MONFAREDI[4] and FARIBORZ MASOUDI[5]

[1]Department of Geography and Geology, University of Salzburg, Hellbrunner Str. 34, A-5020 Salzburg, Austria;
✉farzaneh.shakerardakani@sbg.ac.at
[2]Institute of Isotope Geology and Mineral Resources, ETH Zürich, CH-8092 Zürich, Switzerland
[3]State Key Laboratory of Continental Dynamics, Department of Geology, Northwest University, Northern Taibai Str. 229, Xi'an 710069, China
[4]Institute of Earth Sciences, University of Graz, Universitätsplatz 2, A-8010 Graz, Austria
[5]Faculty of Earth Sciences, Shahid Beheshti University, 19839-63113, Tehran, Iran

(Manuscript received July 4, 2016; accepted in revised form March 15, 2017)

Abstract: In this paper, we present detailed field observations, chronological, geochemical and Sr–Nd isotopic data and discuss the petrogenetic aspects of two types of mafic dykes, of alkaline to subalkaline nature. The alkaline mafic dykes exhibit a cumulate to foliated texture and strike NW–SE, parallel to the main trend of the region. The $^{40}Ar/^{39}Ar$ amphibole age of 321.32±0.55 Ma from an alkaline mafic dyke is interpreted as an indication of Carboniferous cooling through ca. 550 °C after intrusion of the dyke into the granitic Galeh-Doz orthogneiss and Amphibolite-Metagabbro units, the latter with Early Carboniferous amphibolite facies grade metamorphism and containing the Dare-Hedavand metagabbro with a similar Carboniferous age. The alkaline and subalkaline mafic dykes can be geochemically categorized into those with light REE-enriched patterns [$(La/Yb)_N$=8.32–9.28] and others with a rather flat REE pattern [$(La/Yb)_N$=1.16] and with a negative Nb anomaly. Together, the mafic dykes show oceanic island basalt to MORB geochemical signature, respectively. This is consistent, as well, with the $(Tb/Yb)_{PM}$ ratios. The alkaline mafic dykes were formed within an enriched mantle source at depths of >90 km, generating a suite of alkaline basalts. In comparison, the subalkaline mafic dykes were formed within more depleted mantle source at depths of <90 km. The subalkaline mafic dyke is characterized by $^{87}Sr/^{86}Sr$ ratio of 0.706 and positive $\varepsilon_{Nd}(t)$ value of +0.77, whereas $^{87}Sr/^{86}Sr$ ratio of 0.708 and $\varepsilon_{Nd}(t)$ value of +1.65 of the alkaline mafic dyke, consistent with the derivation from an enriched mantle source. There is no evidence that the mafic dykes were affected by significant crustal contamination during emplacement. Because of the similar age, the generation of magmas of alkaline mafic dykes and of the Dare-Hedavand metagabbro are assumed to reflect the same process of lithospheric or asthenospheric melting. Carboniferous back-arc rifting is the likely geodynamic setting of mafic dyke generation and emplacement. In contrast, the subalkaline mafic sill is likely related to the emplacement of the Jurassic Darijune gabbro.

Keywords: mafic dyke, Sanandaj-Sirjan Zone, $^{40}Ar/^{39}Ar$ dating, whole-rock Sr–Nd isotopes, Carboniferous rift, Palaeotethys.

Introduction

The emplacement of mafic dyke swarms exhibits short-lived magmatic events that convey key information on important temporal and chemical constrains for the evolution of the lithospheric mantle and the upper crust into which these basaltic magmas intrude. Mafic dykes are commonly the result of extensional tectonic regimes in a variety of tectonic settings (e.g., Halls & Fahrig 1987; Ernst & Buchan 2001, 2002; Goldberg 2010; Peng et al. 2011; Srivastava 2011; Li et al. 2013; Saccani et al. 2013) and provide valuable information on processes generating large volumes of mafic magmas. Furthermore, mafic dyke swarms can provide essential insights into the nature of mantle sources (e.g., Maurice et al. 2009; Pirajno & Hoatson 2012; Khanna et al. 2013).

In the Sanandaj-Sirjan Zone (SSZ), however, only a few studies have focused on these rocks (e.g., Saccani et al. 2013; Sharifi & Sayari 2013; Deevsalar et al. 2014). For instance, the gabbroic dykes exposed across the Malayer-Boroujerd plutonic complex close to the study area, located 30 km to the north of the Dorud region, are investigated by Deevsalar et al. (2014). The geochemical signature of the dykes from the Malayer-Boroujerd plutonic complex provides insights for the formation of syn-collisional arc related and intraplate late to post-orogenic mafic magmatism, which accords in two main stages including asthenosphere-derived melt, followed by low pressure fractionation and accumulation at high crustal levels. No detailed information on timing of these mafic dykes is available. Further, in the central SSZ, northeast of Golpaygan, alkaline and subalkaline mafic dykes of uncertain age indicate

two generations from the asthenospheric and lithospheric mantle (Sharifi & Sayari 2013).

In West Iran, the Dorud-Azna region in the central part of the Sanandaj-Sirjan metamorphic Zone is characterized by mixed continental (e.g., the Panafrican granitic Galeh-Doz orthogneiss) and oceanic units (e.g., various amphibolites, the Dare-Hedavand metagabbro with a Carboniferous U–Pb zircon age of 314.6±3.7 Ma) and the Middle Jurassic Darijune gabbro (Figs. 1, 2) (Shakerardakani et al. 2015). The Galeh-Doz orthogneiss and similar nearby granitic gneisses derive from a calc-alkaline, metaluminous granite, and is, according to recent U-Pb age dating, Panafrican in age (Nutman et al. 2014; Shakerardakani et al. 2015). The Panafrican basement hosts numerous mafic dykes, which mainly intruded into the granitic Galeh-Doz orthogneiss of the study area (Fig. 2). Nonetheless, the composition, age and the potential metamorphic overprint of these mafic dykes are still poorly known, and geological evidence suggest that these dykes could be potentially related to the Carboniferous Dare-Hedavand metagabbro or the Jurassic Darijune gabbro.

The main objective of the paper is to constrain the petrographic and geochemical signature as well as the age of the mafic dyke swarm, to compare these dykes with different types of mafic rocks in the region and to discuss the age, nature and origin of these dykes as well as their probable genetic relationships. The ultimate goal is to enhance the understanding of the geodynamic setting and significance of these mafic dykes in this central sector of the Sanandaj-Sirjan metamorphic Zone.

Geological setting

The SSZ is one of the major metamorphic/plutonic zones of the Zagros orogenic belt, which is considered a part of the Alpine–Himalayan mountain range. The Zagros orogenic belt resulted from the collision of the African–Arabian continent and the Iranian microcontinent (Berberian & King 1981; Alavi 1994; Mohajjel & Fergusson 2000; Agard et al. 2005, 2011; Hafkenscheid et al. 2006).

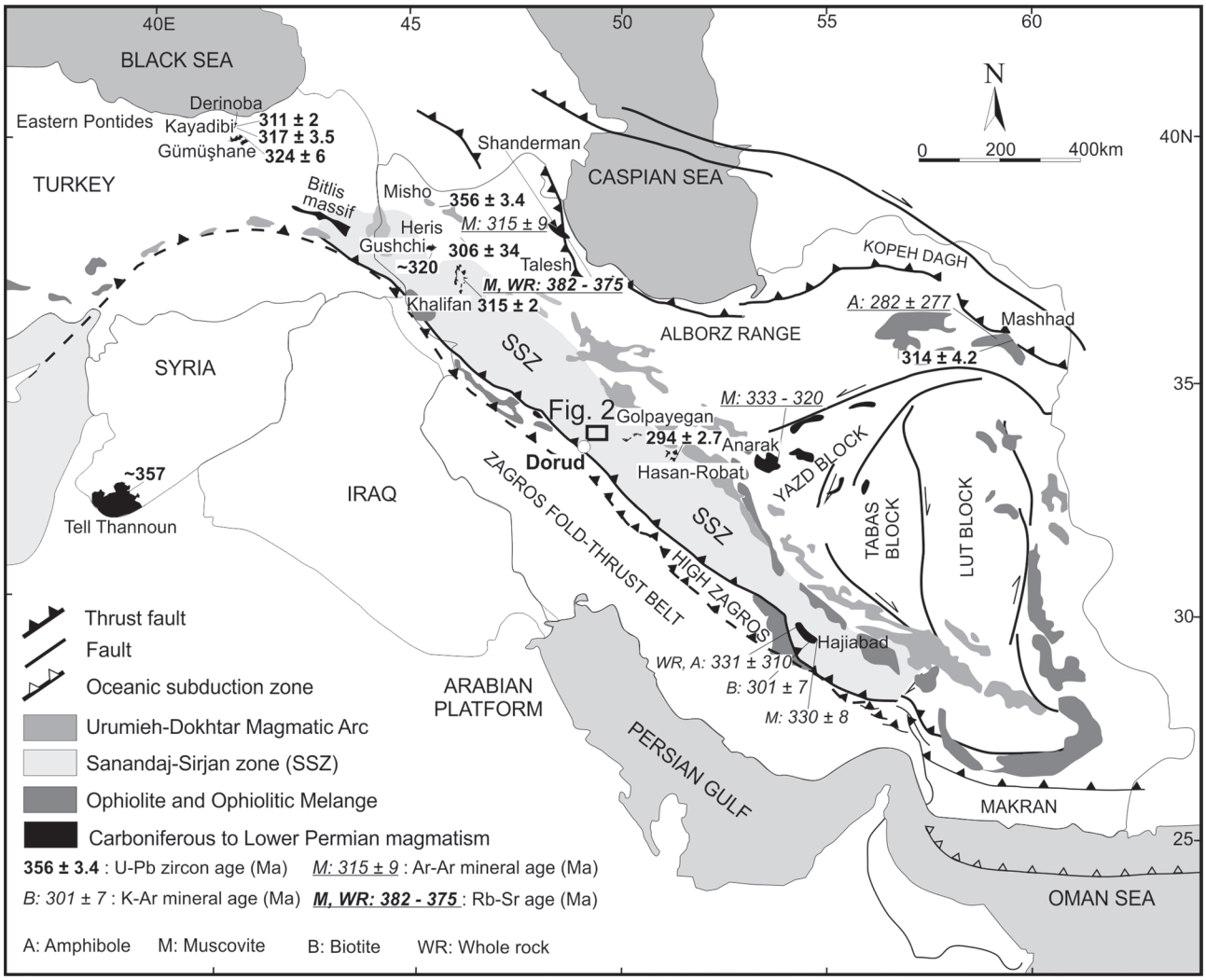

Fig. 1. Simplified geological map of Iran; the black rectangle shows the position of study area. For sources of age dating results, see text.

The Dorud-Azna region is situated in the central part of the SSZ close to the Main Zagros thrust. The structural data combined with the U–Pb zircon dating demonstrated three metamorphosed tectonic units, which include, from footwall to hanging wall: (1) The Triassic June complex is metamorphosed within greenschist facies conditions and is overlain by (2) the amphibolite-grade metamorphic Panafrican Galeh-Doz orthogneiss, which is intruded by mafic dykes, and (3) the

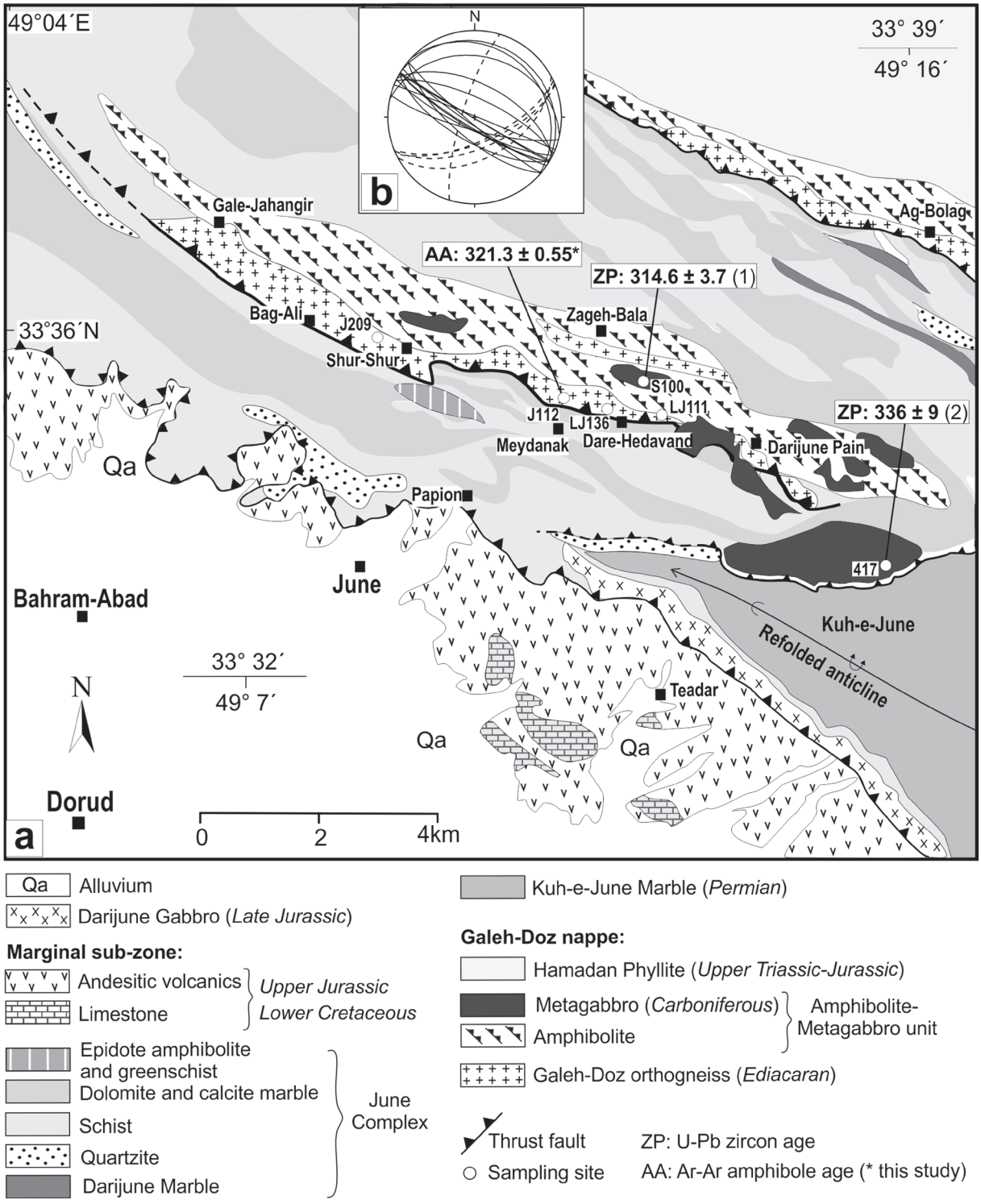

Fig. 2. a — Simplified geological map of the Dorud-Azna region and sample locations of mafic dykes. Ages given in Ma: Data sources: (1) Shakerardakani et al. 2015; (2) Fergusson et al. 2016. Map is updated and modified after Mohajjel & Fergusson (2000). **b** — Orientation of mafic dykes in the Galeh-Doz orthogneiss: alkaline trend mostly WNW–ESE with a variable dip angle whereas subalkaline dykes seem to trend ENE–WSW or NNE–SSW (great circles, 21 data).

Amphibolite-Metagabbro unit, which also includes the Dera-Hedavand metagabbro. To the southeast, these units are intruded by the Darijune gabbro (Shakerardakani et al. 2015). The existence of a Panafrican basement in this part of SSZ has been proposed based on recent U–Pb dating of the granitic Galeh-Doz orthogneiss that yielded ages of 608±18 Ma and 588±41 Ma, respectively (Shakerardakani et al. 2015). The calc-alkaline granitoids of the Panafrican basement were formed during subduction of the Proto-Tethys and are similar to those exposed in Central Iran (Shakerardakani et al. 2015).

In addition, the mafic rocks of the Amphibolite-Metagabbro unit exhibit sub-alkaline to alkaline basaltic compositions, and have an E-MORB geochemistry (Shakerardakani et al. 2015). A laser-ablation ICP-MS U–Pb zircon age of 314.6±3.7 Ma has been reported for the Dare-Hedavand metagabbro from this complex (Shakerardakani et al. 2015) testifying a Late Carboniferous age of gabbro formation. Recently, Fergusson et al. (2016) reported an age of 336±9 Ma for a metagabbro, which was previously undated and considered to be part of the isotropic Darijune gabbro (Shakerardakani et al. 2015).

The metamorphic complex with the Panafrican basement of granitic Galeh-Doz orthogneiss has almost invariably undergone a complex history of repeated shearing, folding, transposition and associated polyphase greenschist- to amphibolite-facies metamorphism (Shakerardakani et al. 2015).

The southeastern part of the study area is intruded by the Darijune gabbro, which stretches over about 5 km in a NW–SE direction. The gabbro body is confined by the presumed Upper Triassic June complex in the north and by the Upper Jurassic to Lower Cretaceous andesitic lavas and pyroclastic rocks in the south. The geochemical and petrographic characteristics of the Upper Jurassic (U–Pb zircon age: 170.2±3.1 Ma) Darijune gabbro indicate a cumulate signature. Shakerardakani et al. (2015) proposed that the cumulate Darijune gabbro was derived from a source highly depleted in incompatible elements, which is interpreted as generated in a continental arc setting.

The studied mafic dykes are located mainly in the centre of the Ediacaran granitic Galeh-Doz orthogneiss. These dykes are characterized by a thickness varying from 0.2 to 4 meters. The majority of dykes strike WNW–ESE and dip steeply to NNE (Fig. 3a). Individual mafic dykes (alkaline dyke; see below) are mostly subvertical, and typically trend NW–SE subparallel to the main trend of the Galeh-Doz orthogneiss. They are mainly foliated with the sharp contact with the host rock (Fig. 3c,d,e). Some dykes and sill-like exposures occur around the Shur-Shur and Dare-Hedavand villages in the central part of the study area (Fig. 2a). Close to Dare-Hedavand these dykes (subalkaline dyke; see below) trend ENE–WSW or NNE–SSW (Fig. 3b). Based on the presence of other mafic magmatic rocks, several potential relationships could be envisaged: (1) The mafic dykes could represent a dyke swarm of the Upper Jurassic Darijune gabbro, (2) the dykes could relate to the Upper Carboniferous Dare-Hedavand metagabbro or, (3) they are derived from none of the mentioned major mafic bodies. Age and geochemical affinities could resolve the open potential relationships.

Petrography

Based on the petrographic evidence as well as geochemical signatures, two groups of mafic dykes are identified in the Dorud-Azna region. The main petrographic features of the mafic dykes of each rock-type are summarized in Table 1. The type i (sample LJ-111) is a subalkaline mafic dyke (see below; Table 1) and show a medium-grained cumulitic texture (Fig. 4a,b). The type ii samples (J-112, J-209, LJ-136) are alkaline mafic dykes and display cumulitic or porphyroclastic textures (Fig. 4c–f). All samples are affected by variable degrees of alteration and/or low-grade metamorphism, what resulted in the partial replacement of primary igneous textures, which are generally well preserved (Fig. 4a–f).

Plagioclase and alkali feldspar grains are mainly altered along the rim and among the cleavage planes, although their textures are preserved in the centre. Chlorite, epidote and sericite are the main secondary minerals after amphibole and plagioclase. The chlorite and epidote displaying various textures of mafic dykes have been metamorphosed at greenschist facies-grade metamorphic conditions with variable preservation of primary magmatic texture.

In one sample (LJ-111), minor amounts of clinopyroxene occur at the margins of amphibole (Fig. 4b). Euhedral to subhedral amphibole is the predominant mineral, whereas euhedral plagioclase and alkali feldspar are subordinate (Fig. 4a, c, d). Chlorite and epidote are the main secondary minerals, although epidote in the one sample (J-112) can be observed as a magmatic mineral (Fig. 4c). Biotite is a fairly common mineral and occurs as a secondary mineral in some samples. Sphene, muscovite, Fe-Ti oxides and apatite represent accessories. Clinopyroxene and the majority of plagioclase grains have been partially replaced by metamorphic or hydrothermal minerals such as epidote, chlorite and sericite. In addition, some fractures in a few samples are filled by secondary calcite and epidote (Fig. 4e).

The strongly foliated alkaline mafic dykes are generally fine- to medium-grained and bear a porphyroblastic texture (Fig. 4f). The major magmatic mineral phases in the mafic dykes are euhedral to subhedral pale- to dark green amphibole, subhedral plagioclase and alkali feldspar, although quartz, and greenish biotite are recognized in this mafic dyke group. The accessory minerals consist of Fe-Ti oxides and apatite.

Analytical methods

Electron Microprobe Analytical Technique

Polished thin sections of samples were analysed using a fully automated JEOL 8600 electron microprobe at the Dept. Geography and Geology, University of Salzburg, Austria. Point analyses were obtained using a 15 kV accelerating voltage and 40 nA beam current. The beam size was set to 5 μm. Natural and synthetic oxides and silicates were used as standards for major elements. Structural formulas for all amphiboles were

calculated according to Holland & Blundy (1994). We used the Mathematica package based software (PET) (Dachs 2004) for mineral formula calculation (including the nomenclature for amphibole according to the IMA scheme), calculation and plotting of mineral compositions.

$^{40}Ar/^{39}Ar$ dating

The $^{40}Ar/^{39}Ar$ techniques largely follow descriptions given in Handler et al. (2004) and Rieser et al. (2006). Preparation of the samples before and after irradiation, $^{40}Ar/^{39}Ar$ analyses,

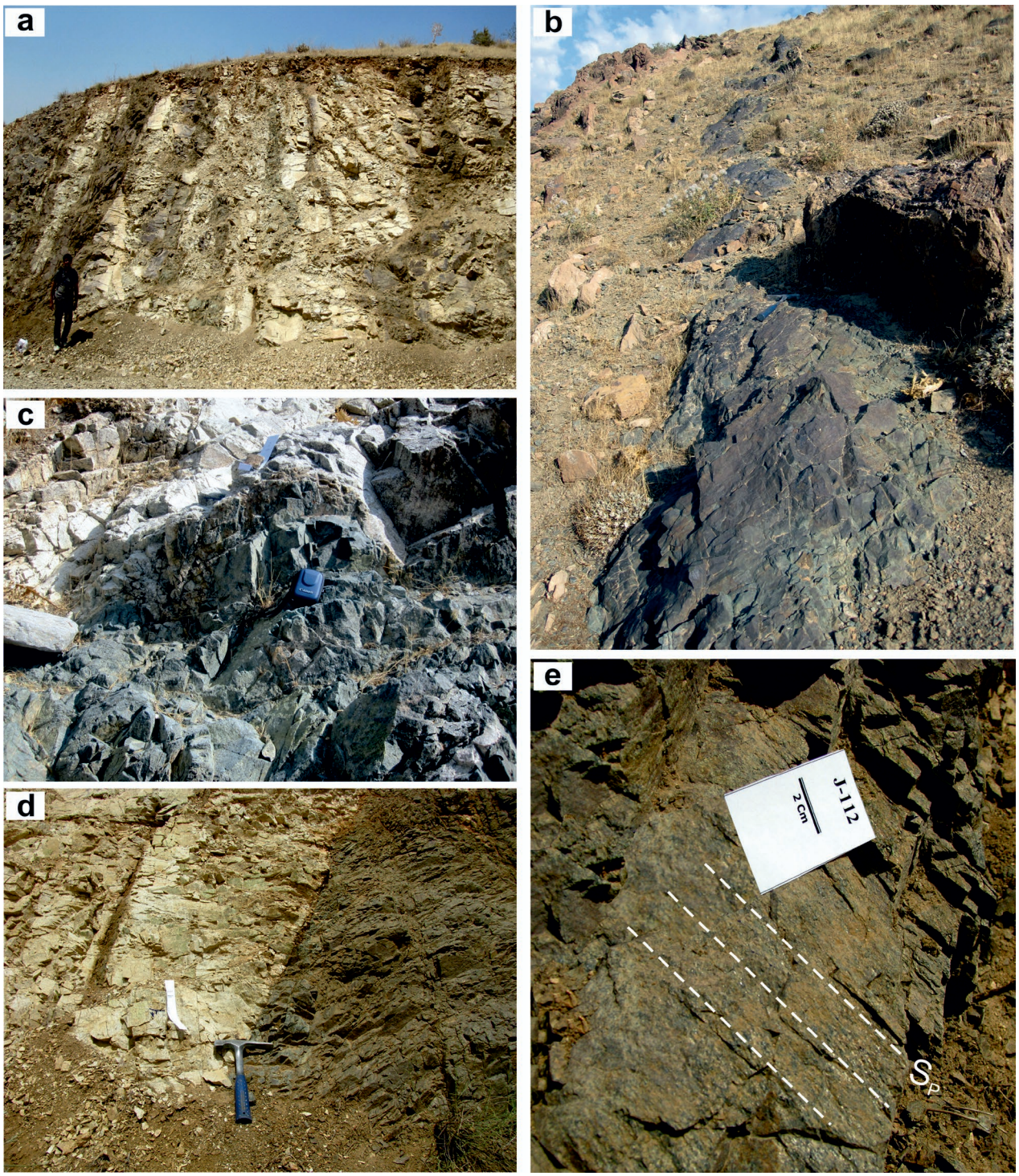

Fig. 3. Field photographs of the mafic dykes in the Dorud-Azna region. Alkaline (**a**), (**b**) mafic dykes trend in the WNW–ESE direction and intruded in the granitic Galeh-Doz orthogneiss and (**c**) metacarbonate. The subalkaline mafic dyke is a sill subparallel to the foliation of the host rock or trend ENE–WSW. **d** — Mafic dykes exhibiting a sharp contact with the host granitic orthogneiss. **e** — Steeply SW-dipping foliation in a mafic dyke.

Table 1: Location, mineralogy and texture of the investigated mafic dyke samples. Abbreviations: pl — plagioclase, kfs — k-feldspar, cpx — clinopyroxene, amp — amphibole, bt — biotite, chl — chlorite, ms — muscovite, spn — sphene, ep — epidote, ser — sericite, qz — quartz, ap — apatite, opq — opaque mineral.

Sample no.	Latitude (°N)	Longitude (°E)	Rock Type	Mineralogy	Texture
LJ-111	33°34'52"	49°11'42"	subalkaline mafic dyke	cpx+amp+pl+kfs+ep+chl+ser+spn+opq+ap	cumulitic texture
J-112	33°35'06"	49°11'04"	alkaline mafic dyke	amp+pl+kfs+ep+chl+bt+qz+ser+spn+opq+ap	cumulitic texture
J-209	33°35'49"	49°08'39"	alkaline mafic dyke	amp+pl+kfs+ep+chl +spn+qz+ms+ser+opq+ap	cumulitic texture
LJ-136	33°34'48"	49°12'02"	alkaline mafic dyke	amp+pl+kfs+ep+chl+ser+spn+opq+ap	highly foliated and porphyroblastic texture

and age calculations were carried out at the ARGONAUT Laboratory of the Department of Geography and Geology at the University of Salzburg. The sample containing primary amphibole was crushed and sieved following standard procedures. By comparison, the 200–350 µm fraction was separated under the microscope. The mineral concentrate was wrapped in Al foil. The sample packet was loaded in 5×5 mm wells on a ~30 mm Al-disk for irradiation, which was done without Cd shielding in the LVR-15 reactor at Rez, Czech Republic, at a thermal neutron fluence of ~4.8×10^{13} n/cm^{2}s and a thermal to fast neutron ratio of ~2.1. All ages were calculated using Fish Canyon sanidine as a flux monitor (28.305±0.036 Ma; Renne et al. 2010). Errors on ages are 1σ. The decay constants used are those given in Renne et al. (2010). Corrections for interfering Ar isotopes were done using $^{36}Ar/^{37}Ar_{(Ca)}$=0.000245, $^{39}Ar/^{37}Ar_{(Ca)}$=0.000932, $^{38}Ar/^{39}Ar_{(Ca)}$=0.01211 and $^{40}Ar/^{39}Ar_{(K)}$= 0.0183 and by applying 5 % uncertainty. Isotopic ratios, ages and errors for individual steps were calculated following suggestions by McDougall & Harrison (1999) and Scaillet (2000). Definition and calculation of plateau ages was carried out using ISOPLOT/EX (Ludwig 2003).

Major and trace element geochemistry

Whole-rock major and trace elements for 4 fresh dyke samples from Dorud-Azna region were determined. Fresh chips of whole rock samples were powdered using an agate mill, and preserved in a desiccator for analysis after being dried in an oven at 105 °C for 2 hours. Major and trace element compositions were analysed by means of XRF (Rigaku RIX 2100) and ICP-MS (PE 6100 DRC), respectively, at the State Key Laboratory of Continental Dynamics, Northwest University, China. For major element analysis, 0.5 g sample powders were mixed with 3.6 g $Li_2B_4O_7$, 0.4 g LiF, 0.3 g NH_4NO_3 and minor LiBr in a platinum pot, and melted to form a glass disc in a high frequency melting instrument prior to analysis. For trace element analysis, sample powders were digested using HF+HNO_3 mixture in high-pressure Teflon bombs at 190 °C for 48 hours. Analyses of USGS and Chinese national rock standards (BCR-2, GSR-1 and GSR-3) indicate that both analytical precision and accuracy for major elements are generally better than 5 %, and for most of the trace elements except for transition metals are better than 2 % and 10 %, respectively. Additionally, one sample was randomly selected to be analysed twice to test the accuracy.

Sr–Nd isotope analysis

Details of the analytical techniques of Rb–Sr and Sm–Nd isotope geochemistry, taking into account their accuracy and precision can be found in von Quadt et al. (1999). For the isotopic analysis, ~50 mg of whole-rock powder was dissolved in HF and HNO_3, followed by Pb, Nd and Sr separation by exchange chromatography techniques on 100 µl TEP columns with Sr Tru and Ln spec Eichrom resin. Nd was purified on a Ln spec column (2 ml) using 0.22 n and 0.45 n HCL. Nd and Sr isotopes were analysed on a ThermoPlus mass spectrometer by static mode measurements at ETH Zürich. Sr was loaded with a Ta emitter on Re filaments. The measured $^{87}Sr/^{86}Sr$ ratios were normalized to an $^{88}Sr/^{86}Sr$ value of 8.37521. The mean $^{87}Sr/^{86}Sr$ value of the NBS 987 standard obtained during the period of measurements was 0.710252±12 (2 σ, n=18). Pb was loaded with a silica gel on Re filaments. A mass fractionation correction of 1.1 ‰ per atomic mass unit was applied, based on replicate analyses of the NBS 982 reference material. Nd was loaded with 2 n HCL on Re filaments. The measured $^{143}Nd/^{144}Nd$ ratios were normalized to the $^{146}Nd/^{144}Nd$ value of 0.7219. The mean $^{143}Nd/^{144}Nd$ value of the Nd Merck standard obtained during the period of measurements was 0.511730±1 (2 σ, n=12). Age-corrected Nd and Sr isotope ratios were calculated using Rb, Sr, Sm and Nd concentrations determined by LA-ICP-MS.

Mineral chemistry

The mafic dykes are classified into two types based on their mineral paragenesis: (i) the mafic dyke comprising clinopyroxene+amphibole+plagioclase+K-feldspar+epidote+chlorite+sphene±opaque minerals+apatite (subalkaline mafic dyke, sample LJ-111) and (ii) the mafic dykes containing amphibole+plagioclase+K-feldspar+quartz+epidote+sphene+chlorite±biotite±muscovite+apatite+opaque minerals (alkaline mafic dykes). In type (i), clinopyroxene is augite (according to Morimoto 1988) with relatively high Mg# (Mg#= 64.5) and FeO (8.84 wt. %), whereas the Al_2O_3 content (0.37 wt. %)

is low (Table 2). Amphiboles show uniform compositions and are mainly magnesio-hornblende with a smaller amount of edenite (Leake et al. 1997) with Mg#=66.11–72.14, Na_2O= 1.1–1.74 wt. % and low K_2O (0.05–0.70 wt. %). In contrast, amphiboles in type (ii) of mafic dykes represent a relatively wide compositional range from hastingsite, magnesio-hastingsite and ferro-edenite to ferro-hornblende, ferro- and tschermakite (Fig. 5). Their Mg# value varies from 39.77 to

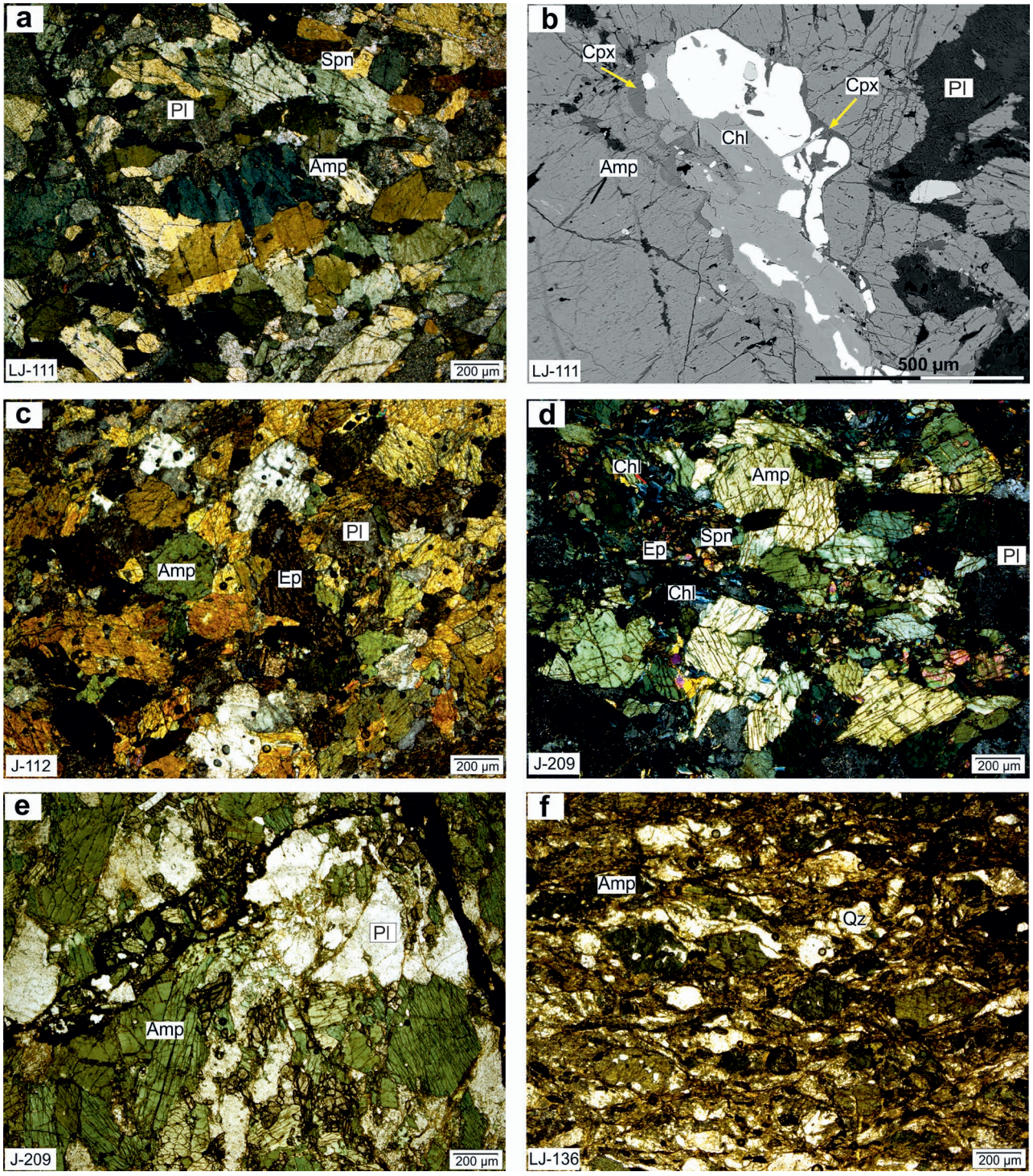

Fig. 4. Representative photomicrographs (a and c–f) and Back-scattered electron (BSE) image (b) of the mafic dykes from the Dorud-Azna region: **a** — The plagioclase is altered to sericite and epidote; **b** — clinopyroxene replaced by amphibole and chlorite; **c, d** — epidote associated with amphibole and sphene; **e** — subparallel fractures filled by epidote and calcite aggregates; **f** — foliated mafic dyke with rounded amphibole porphyroclast and smaller plagioclase porphyroclast in a fine-grained matrix. Amp – amphibole, Pl – plagioclase, Spn – sphene, Cpx – clino-pyroxene, Chl – chlorite, Ep – epidote, Qz – quartz.

Table 2: Representative microprobe analyses of Cpx – clinopyroxene, Amp – amphibole, Ep – epidote, Pl – plagioclase, Kfs – K-feldspar, Mg#=Mg/(Mg+Fe)*100; Ps=Fe^{+3}/(Fe^{+3}+Al)*100.

Sample type	**Subalkaline dyke**												**Alkaline dyke**							
Sample No.	**L J-111**												**L J-136**			**J-209**		**L J-136**		**J-209**
Mineral	Cpx	Amp				Ep		Pl			Kfs		Amp					Ep	Pl	
SiO2	57.11	45.46	46.07	44.96	46.20	37.76	37.72	59.64	60.54	65.36	64.23	63.65	41.07	40.83	42.32	43.84	43.02	38.61	65.72	30.00
Al2O3	0.37	9.89	9.93	10.52	9.54	23.77	23.86	24.40	23.69	20.93	18.26	18.43	10.81	11.25	9.44	10.63	10.00	22.15	21.16	2.58
MgO	18.61	13.00	12.98	12.43	12.19	0.00	0.02	0.00	0.06	0.01	0.00	0.00	6.42	6.51	7.47	6.97	9.08	0.00	0.00	0.01
Na2O	0.04	1.37	1.46	1.70	1.36	0.01	0.00	7.98	8.49	10.27	0.31	0.29	1.61	1.44	1.56	2.00	1.42	0.00	9.96	0.02
CaO	12.99	11.89	11.83	11.85	11.66	23.47	23.31	6.36	4.70	2.14	0.00	0.09	10.94	10.85	10.79	11.48	11.48	22.52	2.41	27.59
TiO2	0.00	0.78	0.87	0.92	0.82	0.04	0.05	0.00	0.00	0.00	0.00	0.03	0.70	0.58	1.01	2.76	0.87	0.06	0.00	34.28
FeO	8.84	13.39	12.88	13.88	13.61	11.01	11.45	0.06	0.28	0.13	0.10	0.06	24.18	23.92	22.50	17.71	20.26	12.59	0.15	1.98
MnO	0.21	0.25	0.26	0.21	0.25	0.05	0.09	0.00	0.01	0.01	0.00	0.01	0.51	0.54	0.56	0.23	0.30	0.19	0.00	0.04
Cr2O3	0.00	0.11	0.08	0.13	0.06	0.02	0.00	0.00	0.00	0.01	0.00	0.00	0.00	0.04	0.01	0.03	0.00	0.01	0.02	0.02
K2O	0.00	0.59	0.59	0.67	0.70	0.00	0.00	0.11	0.77	0.17	16.55	16.38	1.33	1.41	1.03	0.65	1.06	0.00	0.04	0.00
Total	98.26	96.73	96.95	97.30	96.37	96.13	96.53	98.56	98.54	99.04	99.45	98.94	97.59	97.39	96.68	96.34	97.48	96.13	99.46	96.52
Si	2.08	6.75	6.80	6.66	6.87	6.02	6.00	10.78	10.94	11.60	11.97	11.92	6.44	6.41	6.62	6.69	6.59	3.11	11.60	1.02
Al	0.02	1.73	1.73	1.84	1.67	4.48	4.48	5.20	5.05	4.38	4.01	4.07	2.00	2.08	1.74	1.91	1.81	2.10	4.40	0.10
Mg	1.01	2.88	2.85	2.75	2.70	0.00	0.00	0.00	0.02	0.00	0.00	0.00	1.50	1.52	1.74	1.59	2.08	0.00	0.00	0.00
Na	0.00	0.39	0.42	0.49	0.39	0.00	0.00	2.79	2.97	3.54	0.11	0.11	0.49	0.44	0.47	0.59	0.42	0.01	3.41	0.00
Ca	0.50	1.89	1.87	1.88	1.86	4.01	3.97	1.23	0.91	0.41	0.00	0.02	1.84	1.82	1.81	1.88	1.88	0.00	0.46	1.00
Ti	0.00	0.09	0.10	0.10	0.09	0.00	0.01	0.00	0.00	0.00	0.00	0.00	0.08	0.07	0.12	0.32	0.10	0.00	0.00	0.87
Fe	0.27	1.66	1.59	1.72	1.69	1.47	1.52	0.01	0.04	0.02	0.02	0.01	3.17	3.14	2.94	2.26	2.60	0.76	0.02	0.06
Mn	0.00	0.03	0.03	0.03	0.03	0.01	0.01	0.00	0.00	0.00	0.00	0.00	0.07	0.07	0.07	0.03	0.04	0.00	0.00	0.00
Cr	0.00	0.01	0.01	0.01	0.01	0.00	0.00	0.00	0.00	0.00	0.00	0.00	0.00	0.00	0.00	0.00	0.00	0.00	0.00	0.00
K	0.00	0.11	0.11	0.13	0.13	0.00	0.00	0.03	0.18	0.04	3.94	3.91	0.27	0.28	0.21	0.13	0.21	0.00	0.01	0.00
Total	98.17	38.55	38.50	38.62	38.46	41.00	41.00	52.04	52.11	51.99	52.05	52.05	38.86	38.84	38.73	38.39	38.72	8.05	51.91	8.06
Mg#	64.5	72.1	70.1	67.8	66.1								39.77	44.78	41.56	52.81	41.23			
Ps						22.81	23.45											26.62		
X_{Ab}								0.69	0.89	0.92	0.030	0.028							0.880	0.97
X_{An}								0.30	0.10	0.07	0.001	0.000							0.117	0.01
X_{or}								0.01	0.01	0.01	0.969	0.972							0.002	0.03

52.81, and they have large K_2O contents (0.65–1.41 wt. %). Ps contents of the epidote grains in the type (i) are within a narrow range from Ps_{22} to Ps_{23}. The pistacite content in type (i) is higher (Ps_{26}). Plagioclase in type (ii) is mainly albite with the albite content ranging from 88 to 96%. In comparison, the main composition of plagioclase in type (i) is oligoclase ($Ab_{69–88}$) while a minor amount of albite exists (Ab_{92}). Alkali feldspar in these rocks is mainly orthoclase ($Or_{96–97}$) with smaller amounts of anorthoclase and sanidine ($Or_{15–23}$).

$^{40}Ar/^{39}Ar$ dating

Sample J-112, which belongs to type (ii), alkaline dykes (see below), yields a well preserved magmatic amphibole, which is nearly not overprinted by subsequent low-grade metamorphism. The medium-sized amphibole grains together with biotite and feldspar define the stretching lineation and foliation in this peculiar sample. Amphibole grains are commonly replaced by biotite along the micro-fractures and cleavage planes (Fig. 4c). The amphibole grains bear no or only a few inclusions of other mineral phases (Fig. 4c).

The analytical results are given in Table 3 and are graphically shown in Fig. 6. The sample shows some small portion of excess argon in the first step. Steps 4 to 8 (comprising 98.8 % of ^{39}Ar released) yield a plateau age of 321.32±0.55 Ma. Isotopic inversion yields an age of 319.3±1.1 Ma and initial $^{40}Ar/^{36}Ar$ ratio of 262±21 implying the presence of some minor argon loss. We suggest, therefore, that the slightly older

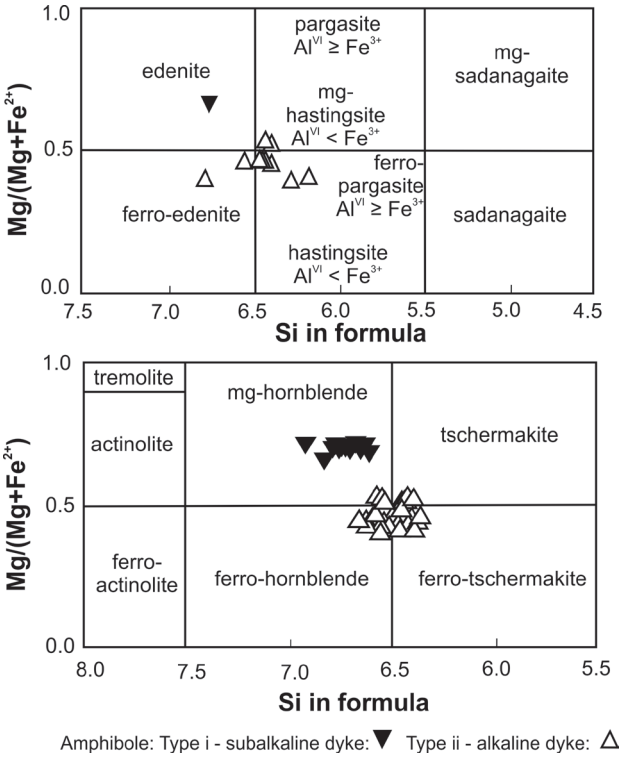

Fig. 5. Composition of amphiboles in the subalkaline and alkaline mafic dykes plotted in the classification diagrams by Leake et al. (1997).

Table 3: Analytical results of $^{40}Ar/^{39}Ar$ amphibole dating of an alkaline mafic dyke in Dorud-Azna region.

step	^{36}Ar meas.	$\pm\sigma_{36}$	^{37}Ar decay corr.	$\pm\sigma_{37}$	^{38}Ar meas.	$\pm\sigma_{38}$	^{39}Ar decay corr.	$\pm\sigma_{39}$	^{40}Ar meas.	$\pm\sigma_{40}$	$^{40}Ar^*/^{39}Ar_K$	$\pm\sigma$	$\%^{40}Ar^*$	$\%^{39}Ar$	age (Ma)	$\pm 1\sigma$ (Ma)	$^{37}Ar_{Ca}/^{39}Ar_K$	$^{38}Ar_{Cl}/^{39}Ar_K$
Sample: J-112, amphibole, 200–355 µm, 7 grains, J-Value: 0.010764 +/– 0.000007																		
1	2.2859E+02	5.24E+00	1.2708E+03	3.11E+01	7.5528E+01	4.19E+00	1.9145E+02	2.26E+01	9.1890E+04	8.65E+01	128.4204	17.2714	26.5	0.1	1566.1	140.8	1577.1	141.5	6.67882	0.11367
2	2.2787E+02	5.63E+00	1.6620E+03	2.11E+01	1.1707E+02	5.08E+00	6.2651E+02	3.03E+01	1.2901E+05	1.51E+02	98.86935	5.49173	47.8	0.3	1307.5	51.7	1317.1	52.0	2.659380	0.08869
3	3.9861E+02	7.59E+00	5.2256E+03	6.74E+01	2.6108E+02	6.75E+00	1.6806E+03	5.24E+01	2.1388E+05	1.83E+02	57.56723	2.24774	44.9	0.8	870.0	27.0	876.8	27.1	3.118483	0.07798
4	1.4318E+02	3.47E+00	7.2780E+04	1.58E+02	4.3167E+03	2.03E+01	1.7337E+04	2.20E+01	3.4337E+05	3.21E+02	17.73671	0.06622	87.7	8.3	315.2	1.1	318.0	1.1	4.214360	0.20806
5	2.8744E+02	3.87E+00	4.1946E+05	8.39E+02	2.7719E+04	6.91E+01	1.1488E+05	1.44E+02	2.1081E+06	1.54E+03	17.93423	0.02815	96.0	55.2	318.4	0.5	321.2	0.5	3.66374	0.20504
6	7.2439E+01	4.01E+00	1.5166E+05	3.96E+02	9.0512E+03	3.72E+01	3.8044E+04	8.91E+01	6.9010E+05	8.56E+02	17.93045	0.05712	96.9	18.3	318.4	1.0	321.2	1.0	4.00145	0.19955
7	2.8930E+01	2.70E+00	3.9272E+04	1.62E+02	2.0750E+03	1.63E+01	8.6876E+03	3.43E+01	1.6099E+05	1.57E+02	17.94778	0.11785	94.7	4.2	318.7	1.9	321.5	1.9	4.53962	0.19684
8	5.4103E+01	3.47E+00	1.0714E+05	2.07E+02	6.5810E+03	3.33E+01	2.6579E+04	5.99E+01	4.8363E+05	3.42E+02	17.95190	0.05758	96.7	12.8	318.7	1.0	321.5	1.0	4.04607	0.20905
9	4.5643E-01	3.49E+00	1.6985E+03	3.06E+01	1.2142E+02	8.09E+00	2.7010E+02	4.33E+01	1.2930E+04	1.45E+02	48.10751	8.67566	99.0	0.1	752.8	111.0	758.9	111.8	6.32561	0.39742

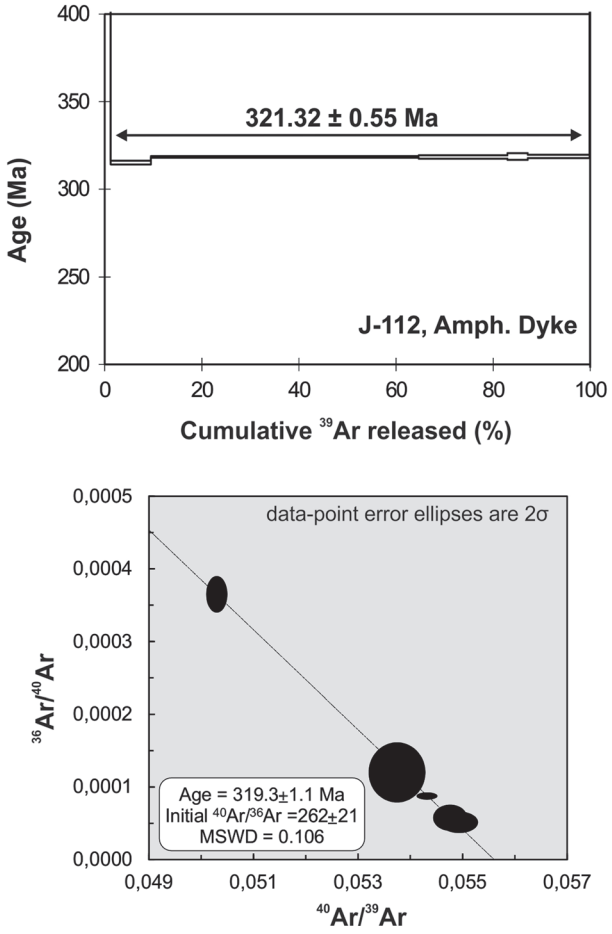

Fig. 6. $^{40}Ar/^{39}Ar$ release pattern of an amphibole concentrate of sample J-112, an alkaline mafic dyke.

plateau age is geologically significant and represents the approximate age of cooling through ca. 550 °C after intrusion of the dyke. As no thermal effects are known, cooling was likely rapid, and the age of 321.32±0.55 Ma is, therefore, close to the real age and represents the approximate age of the intrusion.

Geochemistry

The geochemical results of the four samples of the studied mafic dykes are listed in Table 4. For comparison, these data have been merged in some diagrams with the geochemical data of the Amphibolite-Metagabbro unit and Darijune gabbro from a previous study (Shakerardakani et al. 2015). Note that because of the similar Carboniferous age the isotropic (Darijune) gabbro of the previous study is now merged with the Dera-Hedavand metagabbro. The immobile elements during low-temperature alteration and metamorphism are used for the geochemical features of the mafic rocks. Although, the relative variation of SiO_2, CaO, Al_2O_3 and Fe_2O_3 against immobile elements (e.g., Zr, Y) in a few samples, and also the light and heavy REE (LREE, HREE) elements show good

Table 4: Representative major and trace element analyses of mafic dykes from the Dorud-Azna region.

Sample no.	L J-111	J-112	L J-136	J-209
	Mafic dyke			
	Subalkaline	Alkaline		
SiO_2 wt.%	48.91	46.02	51.02	45.81
Al_2O_3	13.70	12.91	13.45	13.32
Fe_2O_3	10.89	15.29	12.66	14.93
MgO	9.27	5.49	3.31	5.66
CaO	9.53	10.12	7.58	9.52
Na_2O	3.10	3.13	3.90	3.15
K_2O	1.02	1.01	0.91	1.07
TiO_2	1.24	3.48	2.80	3.57
P_2O_5	0.09	0.47	1.25	0.41
MnO	0.17	0.21	0.19	0.19
LOI	2.17	2.10	3.13	2.08
TOTAL	100.09	100.23	100.2	99.71
Mg#	42.33	23.64	18.40	24.64
Li (ppm)	6.63	8.05	13.83	10.09
Be	0.71	2.31	2.85	2.32
Sc	36.41	30.76	21.35	31.35
V	238.8	423.1	220.1	417.1
Cr	386.99	61.91	13.55	51.56
Co	40.17	44.15	17.71	49.57
Ni	167.46	58.72	7.11	55.50
Cu	14.20	84.68	13.01	62.34
Zn	113.32	145.70	122.47	119.28
Ga	16.66	24.24	25.54	23.58
Ge	1.76	1.85	2.28	2.08
Rb	29.17	24.46	34.61	30.15
Sr	209.2	274.6	364.1	435.9
Y	27.79	28.24	47.78	27.71
Zr	34.5	211.9	196.5	202.4
Nb	1.47	40.59	40.79	37.37
Cs	0.39	0.25	2.69	0.30
Ba	198.0	134.8	179.0	228.4
La	4.72	28.43	42.65	25.20
Ce	12.59	64.26	93.13	59.55
Pr	1.73	8.31	12.47	7.83
Nd	8.89	34.43	53.10	33.05
Sm	2.96	7.28	11.34	7.16
Eu	1.06	2.40	3.79	2.41
Gd	4.00	6.76	10.89	6.71
Tb	0.69	0.99	1.57	0.98
Dy	4.59	5.52	8.77	5.46
Ho	1.00	0.99	1.65	0.99
Er	2.88	2.58	4.33	2.57
Tm	0.41	0.35	0.59	0.35
Yb	2.74	2.07	3.48	2.04
Lu	0.40	0.29	0.50	0.29
Hf	1.21	4.85	4.67	4.69
Ta	0.10	2.31	2.43	2.19
Pb	5.64	7.22	3.73	5.97
Th	0.58	2.49	5.09	2.10
U	0.60	1.42	1.75	0.69

correlations with immobile elements that indicate they have not been mobilized during alteration processes. Two different types of mafic dykes can be distinguished based on geochemical features. The two dyke groups are plotted in the basaltic field of the total alkalis-silica diagram (figure not shown). All the mafic dykes are characterized by a narrow range of SiO_2 (45.81–51.02 wt. %), K_2O (0.91–1.07 wt. %) and Na_2O (3.10–3.90 wt. %). Based on Winchester & Floyd's (1977) diagram, the type (i) mafic dykes plot into the subalkaline (sample L J-111), whereas the type (ii) dykes plot into the alkaline field (Fig. 7). The subalkaline sample of type (i) is characterized by moderate MgO (9.27 wt. %), low contents of TiO_2 (1.24 wt. %), P_2O_5 (0.09 wt. %) and total Fe_2O_3 (10.89 wt. %) and Mg# (42.33). Compared with this type (i), the alkaline

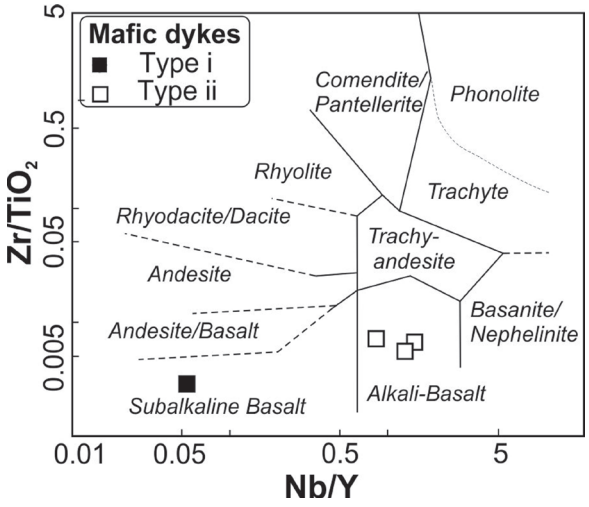

Fig. 7. Nb/Y vs. Zr/TiO_2 diagram for classification of the Dorud-Azna mafic dykes (Winchester & Floyd 1977). Mafic dykes plot in the subalkaline and alkaline fields.

mafic type (ii) dykes consist of an average lower concentration of MgO (3.31–5.66) and higher TiO_2 (2.80–3.57 wt. %), P_2O_5 (0.41–1.25 wt. %) and total Fe_2O_3 (12.66–15.29 wt. %) contents and Mg# (18.40–24.64) (Table 4). The geochemical characteristics of mafic dykes are further explored in chondrite-normalized rare earth- and incompatible trace multi-element variation diagrams (Fig. 8a,b). Although all samples display regularly decreasing normalized patterns from Ba to Yb in the primitive mantle-normalized diagram, they show significant differences between the two types of dykes (Fig. 8a). Unlike alkaline mafic dykes, the subalkaline mafic dyke is characterized by enrichment in LILE (e.g., Cs, Rb, Ba, Pb and K) and Nb and Zr negative anomalies, suggesting that the subalkaline dyke has some arc features (Sun & McDonough 1989; Bezard et al. 2011). Further, no significant Ti anomaly indicates that fractionation of Fe-Ti oxides is not involved in magma genesis (Briqueu et al. 1984). The alkaline mafic dykes have higher REE abundances and are enriched in LREE with $(La/Sm)_N$ and $(La/Yb)_N$ ratios ranging from 2.21 to 2.46 and 8.32 to 9.28, respectively (Fig. 8b), that are similar to those of enriched basalts, such as E-MORBs and OIBs. Although rather low $(La/Yb)_N$ and $(La/Sm)_N$ ratios (1.16 and 1.00 respectively) in the subalkaline mafic dyke imply a source more depleted in LREE than E-MORB. No obvious Eu anomaly (Eu/Eu*=0.94–1.06) in both alkaline and subalkaline mafic dykes indicates that plagioclase was not a major accumulating mineral phase.

Sr-Nd isotopes

Sr and Nd isotopic compositions are presented in Table 5. Mafic dyke samples accompanied by samples of granitic Galeh-Doz orthogneiss, Dare-Hedavand metagabbro from the Amphibolite-Metagabbro unit and Darijune gabbro were subject to Rb–Sr and Sm–Nd isotope analyses too, for com-

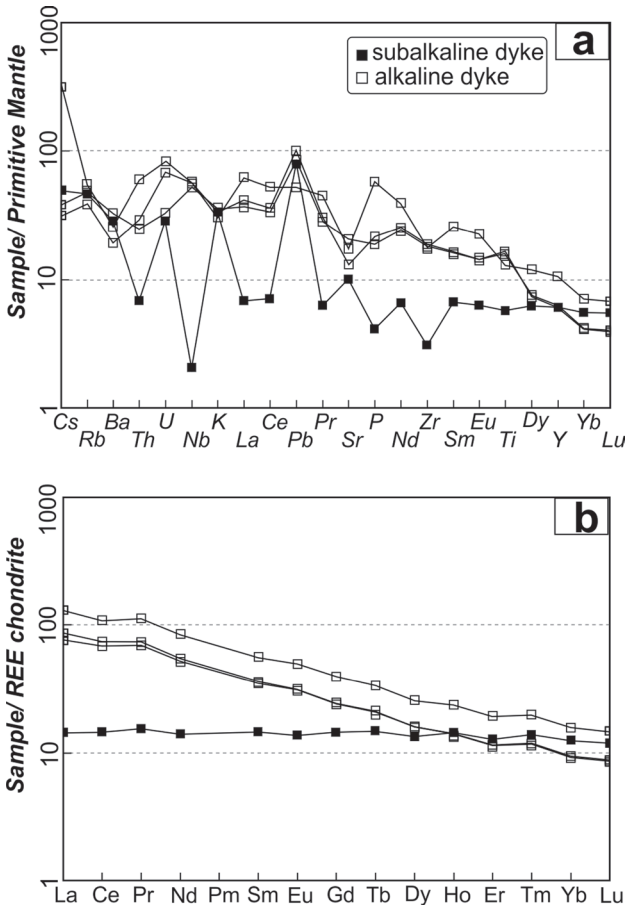

Fig. 8. Chondrite-normalized REE patterns (Boynton 1984) and primitive mantle-normalized incompatible element pattern (Sun & McDonough 1989) for mafic dykes.

parison and further discussion of the origin of mafic dykes. Isotopic data of all samples are plotted in the $^{87}Sr/^{86}Sr_{(i)}$ versus $^{143}Nd/^{144}Nd_{(i)}$ and $^{87}Sr/^{86}Sr_{(i)}$ versus $\varepsilon_{Nd(t)}$ diagrams (Fig. 9a,b).

The subalkaline mafic dyke has an initial $^{87}Sr/^{86}Sr$ ratio of 0.706 and ε_{Nd315} value of +0.77. The alkaline mafic dyke has an initial $^{87}Sr/^{86}Sr$ ratio of 0.708 and ε_{Nd315} value of +1.65, higher than the subalkaline dyke. The higher $^{87}Sr/^{86}Sr$ value observed in alkaline mafic dyke is probably the result of melts with an enriched mantle signature (Fig. 9a, b).

In the Dare-Hedavand metagabbro, initial $^{87}Sr/^{86}Sr$ ratios calculated at 314 Ma (U–Pb zircon age) vary from 0.704 to 0.706 in the isotropic and cumulate metagabbro, respectively. However, the isotropic metagabbros (S-105, LJ-146) have higher values of ε_{Nd314} (+1.66 to +2.58) than cumulate metagabbro (+0.88), which is significantly affected by partial melting/fractionation crystallization processes during generation of the mafic melt (Fig. 9c).

The low initial $^{87}Sr/^{86}Sr$ ratios and the positive ε_{Nd170} value clearly indicate a mantle origin of the Darijune gabbro. The cumulate Darijune gabbro (T-108) also has a low $^{87}Sr/^{86}Sr$ initial ratio (0.7041) and the highest ε_{Nd170} (+5.43) within all the investigated mafic samples, indicating a depleted mantle source.

The Galeh-Doz orthogneiss exhibits a wide range of age-corrected (588 Ma; U–Pb zircon age) $^{87}Sr/^{86}Sr$ initial ratio from 0.704 to 0.707 (Fig. 9a,b), whereas the age-corrected $\varepsilon_{Nd(t)}$ values for these samples define a restricted range from −2.36 to −3.27. In this orthogneiss, $Sr_{(i)}$ ratios increase with increasing SiO_2 (Fig. 9c), indicating that addition of crustal materials (i.e., crustal contamination) likely occurred during magma emplacement (e.g., De Paolo 1981). The presence of inherited zircons in the granitic orthogneiss (Shakerardakani et al. 2015) is also indicative of crustal assimilation or magma hybridization (e.g., Bonin 2004).

Discussion

Pressure and temperature constraints

In order to evaluate the depth of origin of material and the depth of intrusion of the mafic dykes, temperature and pressure were calculated using the PET software (Dachs 2004) based on the hornblende-plagioclase thermometer of Holland & Blundy (1994) and the aluminum-in-hornblende barometer (Hammarstrom & Zen 1986; Hollister et al. 1987) respectively.

The estimated equilibration temperature and pressure for the subalkaline dyke are in the range of 700±25 °C at 5±0.8 kbar. P–T estimate for the alkaline dyke assemblage range from 720±30 °C at 5±1.5 kbar. The temperature estimates for the retrograde stage were obtained using the amount of Al^{iv} base in chlorite of Cathelineau (1988). Estimates range from 332 °C to 187 °C in both subalkaline and alkaline dykes, indicating greenschist facies and sub-greenschist facies conditions during metamorphism and alteration.

Table 5: Sr–Nd isotopic compositions from Galeh-Doz orthogneiss, mafic dyke, Darijune gabbro and Amphibolite-Metagabbro unit.

Sample	Age (Ma)	Rb	Sr	$^{87}Rb/^{86}Sr$	$^{87}Sr/^{86}Sr$	2 σ	I_{sr}	Sm	Nd	$^{147}Sm/^{144}Sm$	$^{143}Nd/^{144}Nd$	2 σ	$e_{Nd}(0)$	$e_{Nd}(t)$
G-112	588±41	5.59	75.9	0.2078	0.70714	0.000022	0.70888	11.0	51.4	0.1349	0.512289	0.000009	−6.81	−2.369
L J-112	588±41?	107	161	1.8775	0.70401	0.000055	0.71975	7.84	37.4	0.1319	0.512231	0.000006	−7.94	−3.274
J-112	321±0.55	24.5	275	0.2513	0.70803	0.000054	0.70915	7.28	34.4	0.1331	0.512592	0.000003	−0.90	1.653
L J-111	321? or 170?	29.2	209	0.3935	0.70653	0.000045	0.70829	2.96	8.89	0.2101	0.512705	0.000012	1.31	0.771
T-108	170±3.1	4.16	90.3	0.1301	0.70411	0.000019	0.70442	1.03	2.97	0.2189	0.512941	0.000018	5.91	5.431
L J-146	170±3.1	25.2	452	0.1576	0.70474	0.000032	0.70512	6.66	30.4	0.1379	0.512602	0.000017	−0.70	0.574
S-100	314±3.7	0.55	114	0.0137	0.70500	0.000016	0.70507	2.94	13.0	0.1425	0.512572	0.000032	−1.29	0.886
S-105	314±3.7	6.28	452	0.0392	0.70626	0.000029	0.70644	3.77	13.2	0.1790	0.512734	0.000005	1.87	2.583

Magma generation

The normalized multi-element and REE patterns of the subalkaline and alkaline mafic dykes suggest that the magmas were derived from a mantle source between MORB and OIB-like composition, respectively (Fig. 8). However, low Cr and Ni concentrations in alkaline mafic dykes (13–61 and 7–58 ppm) indicate that these are not primary magmas and underwent some crystal fractionation most likely of spinel, olivine and clinopyroxene. The Al_2O_3/TiO_2 against Ti diagram, which is used as an indicator of differentiation, shows that the mafic dyke as well other investigated mafic groups are mainly characterized by the crystallization of plagioclase+clinopyroxene in the relatively less evolved rocks followed by the crystallization of Fe-Ti-oxides in the more evolved rocks (Fig. 10a). However, it must be noted that it is sometimes difficult to differentiate between the effects of fractional crystallization on the compositions of primary magmas and those of partial melting. A steep trend in the La/Yb vs. La diagram (Fig. 10b) suggests that the effects of partial melting and source composition were more important than fractional crystallization in controlling the compositional variation between the two groups of mafic dyke (e.g., Jiang et al. 2005). In addition, the budget of the moderately incompatible elements (for example, La/Yb, Fig. 10b) in the Dare-Hedavand metagabbro

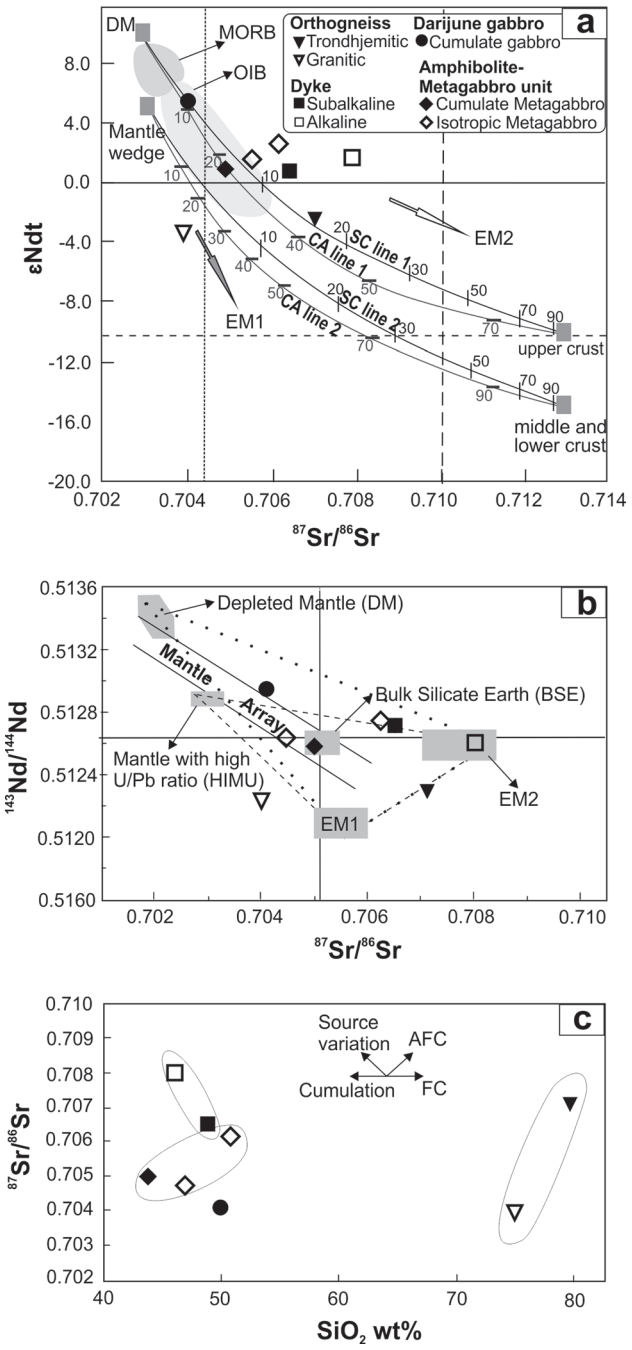

Fig. 9. a, b — Sr–Nd isotopic composition of the mafic dykes with representatives of country rocks including the Panafrican granitic Galeh-Doz orthogneiss, Carboniferous metagabbro and Jurassic Darijune gabbro (data from Shakerardakani et al., 2015). MORB: Mid-Ocean Ridge Basalts; OIB: Ocean Island Basalts; EM1: enriched mantle 1; EM2: enriched mantle 2. **c** — Plot of $Sr_{(i)}$ vs. SiO_2. Note that magmatic rocks of different crystallization ages are plotted together.

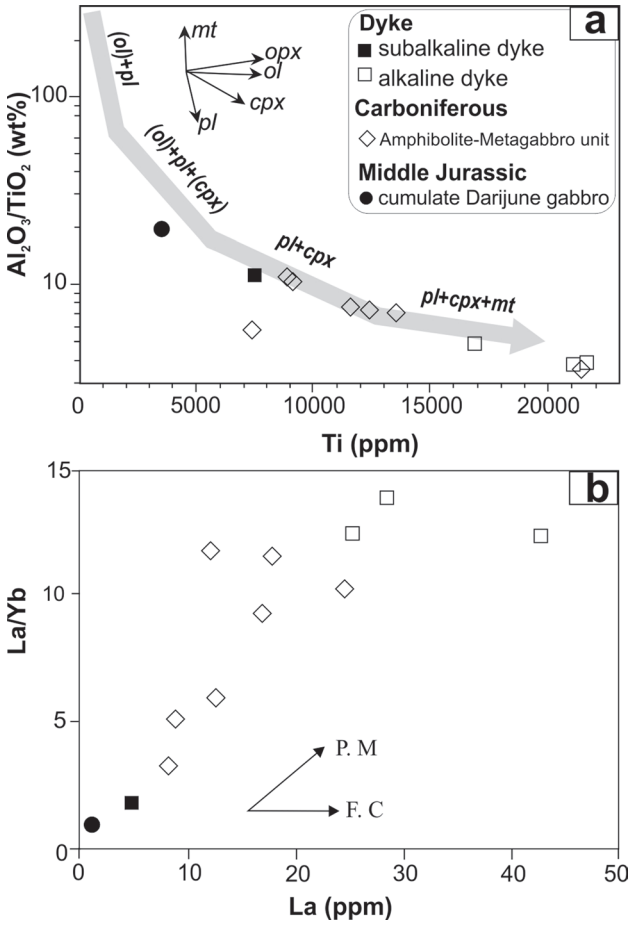

Fig. 10. a — Al_2O_3/TiO_2 vs. Ti diagram for mafic dykes from the Dorud-Azna region. Fractional crystallization (F. C.) vectors of magnetite (mt), orthopyroxene (opx), olivine (ol), clinopyroxene (cpx), and plagioclase (pl) are shown. Modified after Saccani et al. (2013). Arrow shows the estimated fractionation trend. **b** — La/Sm vs. La diagram for the mafic dykes. Vector arrows show the effect of increasing degrees of partial melting (P. M.) and fractionation (F. C.).

is largely controlled by partial melting processes rather than crystal fractionation. Compared with subalkaline magmas, the magma that produced the alkaline mafic dykes probably experienced subsequent fractionation after partial melting (Fig. 10b). These samples reveal a remarkable negative correlation of MgO, Al_2O_3 and Ni with increasing Zr contents and positive correlation of LREE, HREE and Nb (Fig. 11). These patterns are consistent with the fractionation of olivine, pyroxene and plagioclase (Ordóñez-Calderón et al. 2011). Furthermore, the positive correlation between TiO_2 and Zr contents (Fig. 11) could suggest that Fe-Ti oxides minerals were not significant mineral phase during fractionation (Ordóñez-Calderón et al. 2011; Deng et al. 2013).

In order to constrain the geochemical characteristics of the possible mantle sources for the two different types of mafic dykes together with previously investigated mafic rocks, some hygromagmatophile element ratios (e.g., Tb/Yb, La/Sm) have been used. In the $(Tb/Yb)_{PM}$ vs. $(La/Sm)_{PM}$ diagram (Fig. 12a), there are two distinct groups indicating that partial melting played an important role in the chemical compositions of investigated mafic rocks.

High Tb/Yb ratios (2.06–2.20) of the alkaline mafic dykes reflect a deep melting level in the stability field of the garnet-peridotite mantle likely at a depth of more than 90 km, whereas the subalkaline mafic dyke has a lower Tb/Yb ratio (1.15) indicative for melting of shallower spinel-peridotite mantle at a depth of less than 90 km (Wang et al. 2002; Khudoley et al. 2013). In comparison, Tb/Yb and La/Sm ratios of the source region of Dare-Hedavand metagabbros range from 1.30 to 2.08 and 1.40 to 2.65, suggesting they were produced through various degrees of partial melting and/or point to a stronger enrichment of their mantle source. Moreover, lower La/Sm ratios in the subalkaline mafic dyke as well as the cumulate Darijune gabbro than in other mafic groups can be also caused by melting of a depleted source. In contrast, increased partial melting or crustal contamination can enhance the La/Sm ratios. In fact, the magma ascending through continental crust raises the possibility that crustal contamination may have

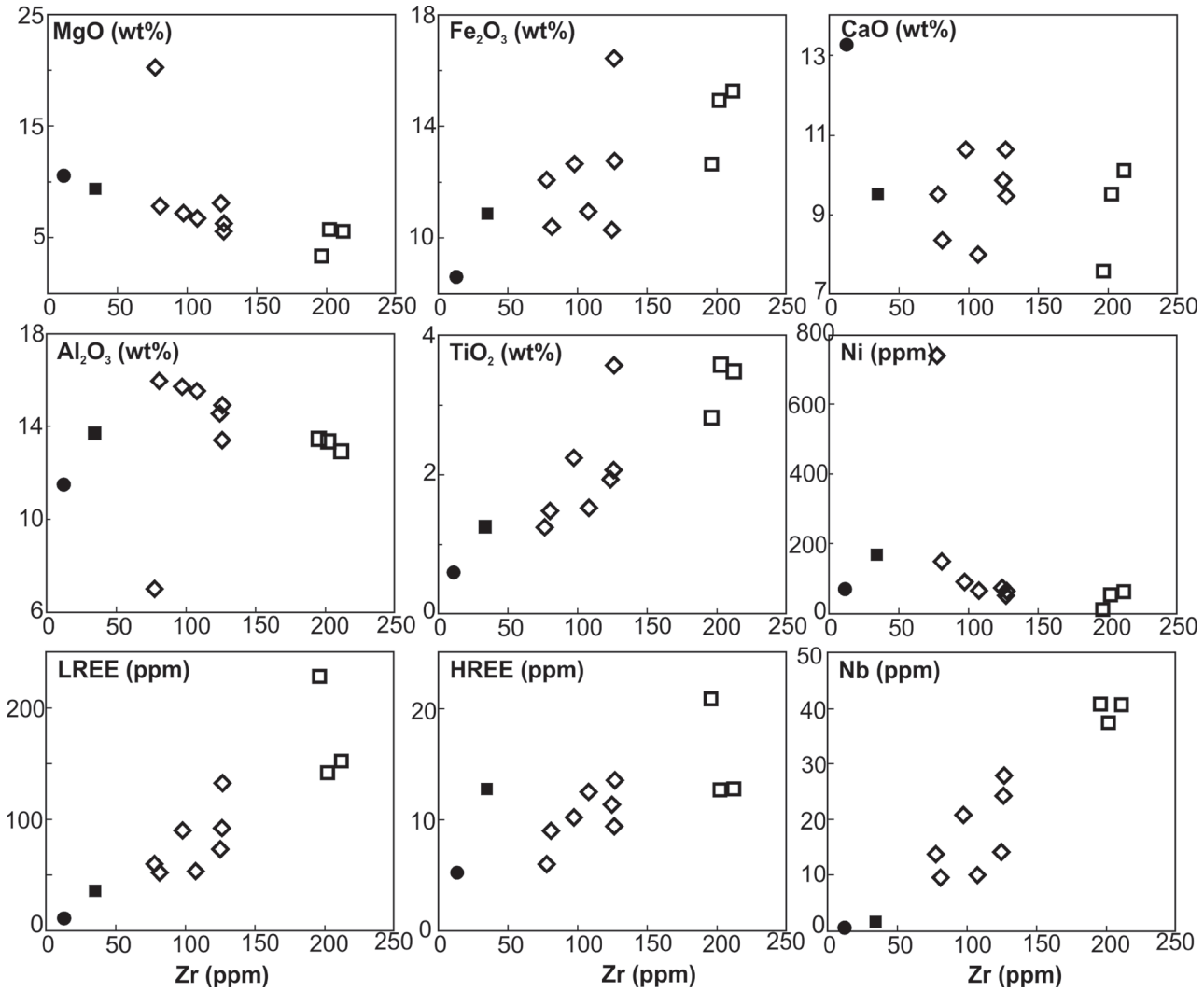

Fig. 11. Variation diagrams of Zr versus the major and trace elements for mafic dykes of the Dorud-Azna region. The data compared with the geochemical data of mafic samples from Amphibolite-Metagabbro unit and Darijune gabbro. Symbols are the same as in Fig. 10.

caused some of the compositional characteristics of the mafic rocks. In respect of the $(Th/Yb)_{PM}$ vs. $(Nb/Yb)_{PM}$ diagram, all distinct groups are in the field of mantle-derived melts (Fig. 12b), suggesting that chemical influence of the continental lithosphere component was very limited or absent, as also supported by the plot in the Nb/La versus Nb/Th diagram (Fig. 12c). For the subalkaline mafic dyke, the initial $^{87}Sr/^{86}Sr$ ratios is negatively correlated to SiO_2, suggesting that crustal contamination plays a minor role in its genesis (Fig. 9c) (e.g., Lin et al. 1990). Therefore, the differences in La/Sm ratios can refer to a differing degree of partial melting and/or magma source. It is assumed that alkaline mafic dyke magmas were produced from a garnet-bearing enriched mantle source (high Tb/Yb ratio) from the deeper source, while the magmas of subalkaline mafic dykes were generated in the shallow and depleted mantle source (low Tb/Yb ratio).

Tectonic implications

The E-MORB and OIB-type affinities of the mafic dykes are typically found in tectonic settings including oceanic-island/seamounts, continental-rifts and some flood-basalt provinces (e.g., Hochstedter et al. 1990; van Staal et al. 1991; Goodfellow et al. 1995; Shinjo et al. 1999; Leitch & Davies 2001). Their genesis has mostly been attributed to mantle plumes, however, there are also occurrences where no plume has been involved (e.g., Haase & Devey 1994).

The geochemical signatures of mafic dykes, accompanied by the various mafic rock types in the Dorud-Azna region indicate that magmas of at least two different compositions originated from mantle sources in various time intervals. The tectonic discrimination diagrams and Sr- and Nd isotopes provide the broadest insight into the setting of this magmatism.

In the ternary Nb–Hf–Th diagram of Wood (1980), alkaline mafic dykes plot in the field of within-plate alkaline basalts, whereas the subalkaline dyke plots within the volcanic-arc basalt field (Fig. 13a). The Dare-Hedavand metagabbro samples demonstrate the alkaline field, similar to alkaline mafic dykes, along with enriched mid-ocean ridge basalt (E-MORB) field. Because of the geochemical similarities and similar protolith ages, we assume a common origin of the alkaline mafic dykes and the Dare-Hedavand metagabbro.

The cumulate Darijune gabbro plots in the field of volcanic-arc basalt. Furthermore, the variation of Ti/V ratio is clearly shown on the Ti/1000 vs. V diagram (after Shervais 1982) that all the samples show transitional signatures, where the subalkaline mafic dyke with a lower Ti/V ratio than the alkaline dykes indicates MORB-affinity magmatism, the mafic dykes as within-plate basalts (not shown), as well as mafic rocks from the Amphibolite-Metagabbro unit plot in the MORB-BAB (back-arc basin) fields overlapping with ocean island alkaline basalts (Fig. 13b).

In the Nb/Yb versus Th/Yb tectonic discrimination diagram of Pearce (2008), all the alkaline mafic dykes and various mafic rocks of the Amphibolite-Metagabbro unit plot along the enriched part of the MORB-OIB array (Fig. 13c). The subalka-

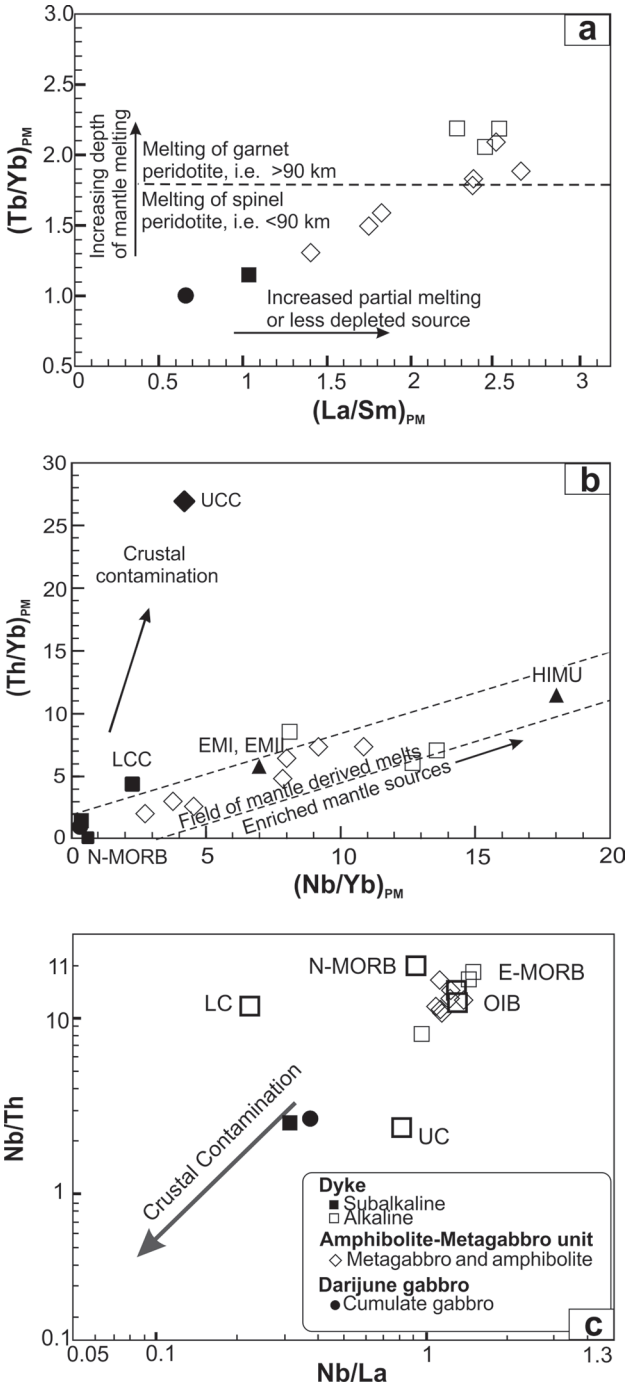

Fig. 12. Variation diagrams for incompatible trace elements and element ratios for different magma compositions after Khudoley et al. (2013). **a** — $(Tb/Yb)_{PM}$ vs. $(La/Sm)_{PM}$ diagram display two distinct groups of mafic dykes; the discrimination line between magmas sourced from melting of spinel peridotite mantle and garnet peridotite mantle is based on Wang et al. (2002). **b** — $(Nb/Yb)_{PM}$ vs. $(Th/Yb)_{PM}$ diagram displaying all samples plot within the field of mantle-derived melts marked with two different ranges; Upper Continental Crust (UCC) and Lower Continental Crust (LCC) compositions are from Taylor and McLennan (1985), and enriched mantle (EMI, EMII) and HIMU (high μ where $\mu=^{238}U/^{204}Pb$) mantle values are from Condie (2001). PM denotes normalization to Primitive Mantle values of McDonough & Sun (1995). **c** — Nb/La vs. Nb/Th diagram showing the trend of crustal contamination (after Zhang et al. 2014).

line mafic dyke plots on a trend toward the area above the mantle array in the arc-back-arc field. On the Zr/Y–Nb/Y diagram (Fitton et al. 1997), the mafic dykes as well as all other investigated mafic rocks groups plot above the ΔNb line [ΔNb=1.74+log(Nb/Y)−1.92 log(Zr/Y)], inside of the plume field (Condie 2005) at relatively high Zr/Y values within the OPB (oceanic plateau basalt) and OIB fields. However, the subalkaline mafic dyke plots within depleted mantle with lower Zr/Y values (Fig. 13d). Consequently, the subalkaline mafic dyke is potentially related to the Darijune gabbro.

Concluding remarks

The REE patterns and some incompatible element ratios reflect the geochemical diversity of the mantle sources prior to the effects of subduction and display that the Dorud-Azna mafic dykes, like metagabbros and Darijune gabbro contain variable mixtures of depleted lithosphere mantle and enriched (OIB-like) asthenospheric mantle sources. These geochemical signatures for mafic dykes support the probably arc-related or plume-related setting. In addition, the $^{40}Ar/^{39}Ar$ amphibole plateau age of ca. 321.32±0.55 Ma of an alkaline mafic dyke demonstrates the potentially similar origin as for the Carboniferous Dare-Hedavand metagabbro and a close genetic relationship between these two types of rock types is, therefore, assumed, probably reflecting the same process of lithospheric or asthenospheric melts for their magma generation. A relationship of the alkaline mafic dykes to the Jurassic Darijune gabbro can be excluded because of difference in age and geochemical composition, although the geochemical signatures (e.g., uprising from a depleted MORB-type asthenosphere) of the subalkaline mafic dyke illustrate a possible relationship with the cumulate Jurassic Darijune gabbro. In this case, the alkaline dyke magma formed together with the Dare-Hedavand metagabbro.

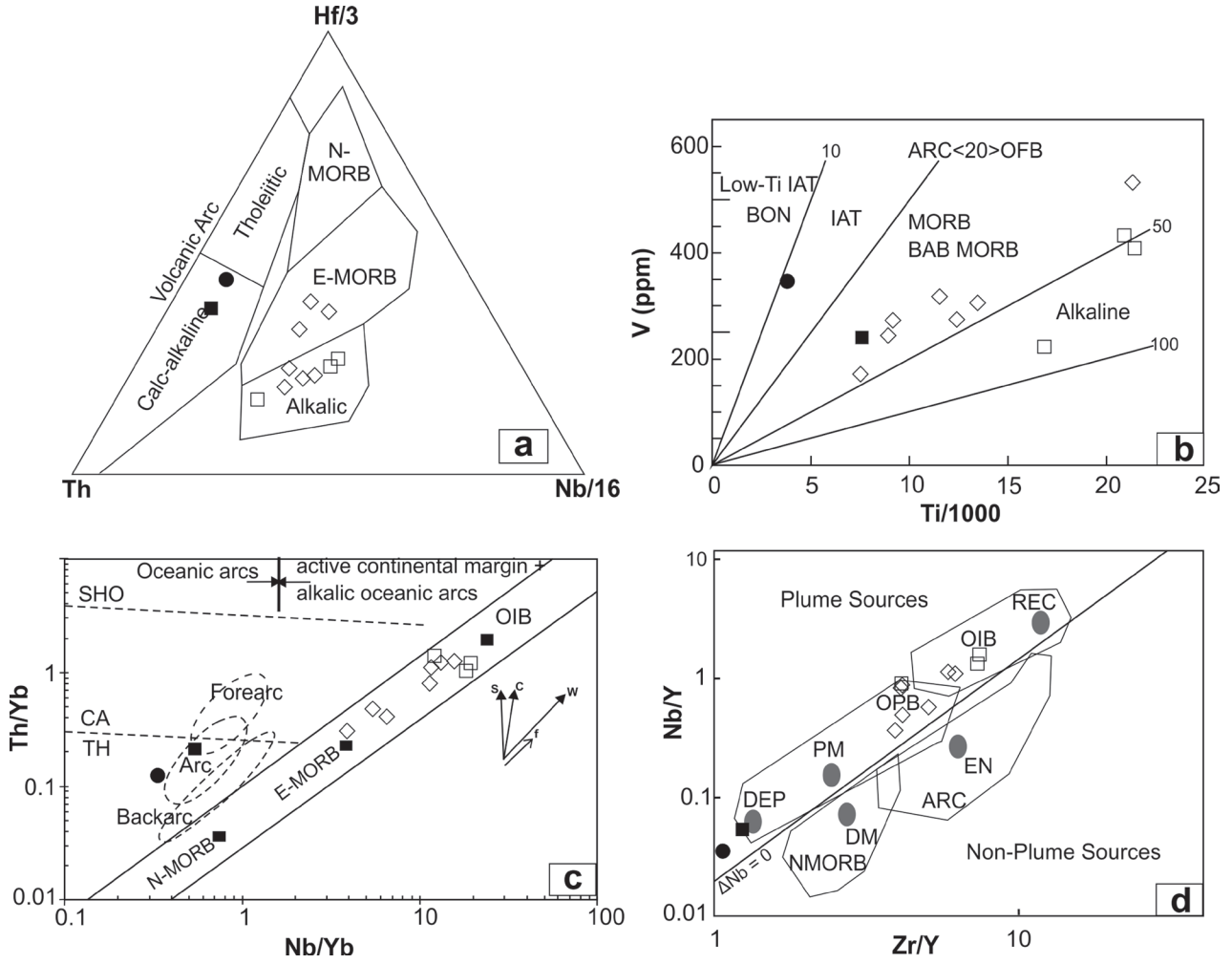

Fig. 13. Tectonic discrimination diagrams. **a** — V vs. Ti/1000 diagram after Shervais (1982); **b** — Hf–Nb–Th plot, with fields defined by Wood (1980); **c** — Nb/Yb versus Th/Yb after Pearce (2008). The dashed field boundaries for TH: tholeiitic, CA: calc-alkaline, and Sh: shoshonitic rocks are from convergent margins. The bold arrows in the bottom right are S: subduction component, C: crustal contaminant component, W: within plate, and f: fractional crystallization vectors; **d** — Zr/Y–Nb/Y diagram (Fitton et al. 1997); DEP: deep depleted mantle; PM: primitive mantle; DM: shallow depleted mantle; EN: enriched component; REC: recycled component; OPB: oceanic plateau basalt; OIB: ocean island basalt; ARC: arc related basalt; NMORB: normal ocean ridge basalt (Symbols are as in Fig. 12).

Carboniferous back-arc rifting seems to be, therefore, the most likely geodynamic setting for alkaline mafic dyke generation and emplacement. It has to be noted that more and more evidence for Carboniferous and earliest Permian magma generation appear both in the Sanandaj-Sirjan Zone and Central Iran, as well as the Alborz range and NE Iran (Fig. 1). In particular, Berberian & King (1981) suggested that Devonian-Carboniferous basalts along the Sanandaj-Sirjan Zone are clearly subjected to a rift setting during the Early Devonian and Carboniferous extensional phase. Recently, Ayati (2015) reported an alkaline to tholeiitic affinity of latest Devonian basalts, for example, from the western Yazd block (Fig. 1), which derived from a deep-seated source potentially indicating initial stages of rifting.

However, in the last decade, more and more evidence has appeared for the existence of Carboniferous to earliest Permian orogenic events in Central Iran (Bagheri & Stampfli 2008; Zanchi et al. 2009a and b; Buchs et al. 2013; Kargaranbafghi et al. 2015), in the Sanandaj-Sirjan Zone (Advay & Ghalamghash 2011; Bea et al. 2011; Moghadam et al. 2015) but also in the Eastern Pontides in Turkey (Topuz et al. 2010; Kaygusuz et al. 2012) and in the northern part of the Arabian plate (Tavakoli-Shirazi et al. 2013; Frizon de Lamotte et al. 2013; Stern et al. 2014). Within the Palaeotethys, Bagheri & Stampfli (2008) postulated "Variscan" terrane accretion in Central Iran, also supported by abundant "Variscan" detritus in Mesozoic sediments of Central Iran (Kargaranbafghi et al. 2015). In addition, evidence from northern (Talesh Mountains) and northeastern Iran (Mashhad-Fariman area) indicate the presence of a Late Palaeozoic, mainly Carboniferous active margin of the Palaeotethys, which is the same as in Central Iran (Nakhlak-Anarak units) developed during the Eo-Cimmerian orogenic cycle (Ghazi et al. 2001; Zanchi et al. 2009a; Zanchetta et al. 2009, 2013). Within the SSZ, U–Pb zircon ages of Gushchi A-granites and gabbronorites in NW Iran indicate that the gabbronorites and granites were emplaced synchronously at ~320 Ma (Moghadam et al. 2015). Saccani et al. (2013) report a U–Pb zircon age of 356.7±3.4 Ma (Early Carboniferous) from a leucogabbro dyke within the Misho Mafic Complex (Fig. 1), which shows N- and P-MORB affinities. Bea et al. (2011) found that the Khalifan pluton of northwestern SSZ includes an A-type peraluminous leucogranite with an intrusion age of 315±2 Ma. Honarmand et al. (2017) found an Early Permian age (294.6±2.7 Ma) for the Hasan-Robat A-type granite. In the southeastern part of the Sanandaj-Sirjan Zone, in the west of Hajiabad, Ghasemi et al. (2002) show Late Carboniferous $^{40}Ar/^{39}Ar$ mineral ages ranging from 330 to 300 Ma. Further, K/Ar ages of 310±9 and 331±5 Ma are reported by Sheikholeslami et al. (2003) in the Neyriz area. All this evidence argues that Carboniferous mafic magmatic complexes are widespread in NW Iran (Fig. 1) and are locally associated with Carboniferous to earliest Permian A-type anorogenic granites. We suggest, therefore, that a major, potentially plume-related rift event is common in NW Iran and it is potentially related to mafic flood basalt magmatism in the northernmost Arabian plate (Stern et al. 2014). The alkaline mafic dykes and the Dare-Hedavand metagabbro from the Dorud–Azna region in the central SSZ are the southernmost occurrences of the mafic anorogenic magmatism within the SSZ and predate the suggested main stage Permian rifting of the SSZ (Hassanzadeh & Wernicke 2016). Our preferred interpretation is that the alkaline dykes of the Dorud-Azna region formed during an initial stage of potentially plume-related rifting and are associated with the intrusion of the Dare-Hedavand metagabbros (Fig. 14). The plume might have induced heating and partial melting of the lithospheric base. Heating also resulted in surface uplift. Overheated mafic magma chambers at the base of the crust might have caused melting of continental crust resulting in A-type granites.

Furthermore, Kohn et al (1992) found a Late Devonian–Early Carboniferous thermo-mechanical event that they related to the "Variscan" orogeny, which is also known in the study area (Shakerardakani et al., submitted). A so-called "Hercynian unconformity" exists everywhere in the Arabian plate (Frizon de Lamotte et al. 2013 and references therein). This deformation and the associated "thermal event" are probably independent from the "Variscan" orogeny in Europe and are rather related to anorogenic magmatic events within the Arabian plate and NW Iran (Frizon de Lamotte et al. 2013; Tavakoli-Shirazi et al. 2013; Stern et al. 2014; Moghadam et al. 2015). Consequently, we suggest that mafic magmatism postdates the rising evidence for "Variscan" orogenic processes in the SSZ and Arabian plate.

Acknowledgements: This paper is part of the PhD thesis of Farzaneh Shakerardakani. FS acknowledges support through a scholarship from the Afro-Asiatisches Institute Salzburg for her PhD thesis at Salzburg University.

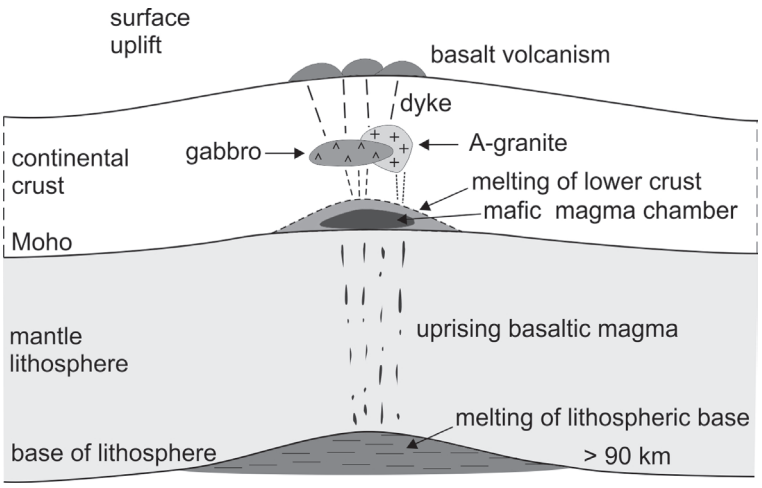

Fig. 14. Simplified tectonic model with the interpretation of formation of Carboniferous alkaline mafic dykes and associated Dera-Hedavand metagabbro due plume tectonics predating rifting.

References

Advay M. & Ghalamghash J. 2011: Petrogenesis and U–Pb dating zircon of granites of Heris (NW of Shabestar), eastern Azerbaigan province. *Iran. J. Crystallogr. Mineral.* 4, 633–648.

Agard P., Omrani J., Jolivet L. & Mouthereau F. 2005: Convergence history across Zagros (Iran): constraints from collisional and earlier deformation. *Int. J. Earth Sci.* 94, 401–419.

Agard P., Omrani J., Jolivet L., Whitchurch H., Vrielynck B., Spakman W., Monie P., Meyer B. & Wortel R. 2011: Zagros orogency: a subduction-dominated process. Cambridge University Press. *Geol. Mag.* 148, 692–725.

Alavi M. 1994: Tectonics of the Zagros orogenic belt of Iran: New data and interpretations. *Tectonophysics* 229, 211–238.

Ayati F. 2015: Geochemistry, petrogenesis and tectono-magmatic setting of the basic magmatism in Ardekan and Isfahan, Central Iran. *J. Afr. Earth Sci.* 108, 64–73.

Bagheri S. & Stampfli G.M. 2008: The Anarak, Jandaq and Posht-e-Badam metamorphic complexes in central Iran: New geological data, relationships and tectonic implications. *Tectonophysics* 451, 123–155.

Bea F., Mazhari A., Montero P., Amini S. & Ghalamghash J. 2011: Zircon dating, Sr and Nd isotopes, and element geochemistry of the Khalifan pluton, NW Iran: Evidence for Variscan magmatism in a supposedly Cimmerian superterrane. *J. Asian Earth Sci.* 44, 172–179.

Berberian M. & King, G.C.P. 1981: Towards a paleogeography and tectonic evolution of Iran. *Can. J. Earth Sci.* 18, 210–265.

Bezard R., Hébert R., Wang C., Dostal J., Dai J. & Zhong H. 2011: Petrology and geochemistry of the Xiugugabu ophiolitic massif, western Yarlung Zangbo suture zone, Tibet. *Lithos* 125, 347–367.

Bonin B. 2004: Do coeval mafic and felsic magmas in post-collisional to within-plate regimes necessarily imply two contrasting, mantle and crustal, sources? A review. *Lithos* 78, 1–24.

Boynton W.V. 1984: Cosmochemistry of the rare earth elements: meteorite studies. In: Henderson P (eds) Rare Earth Element Geochemistry. Elsevier, Amesterdam, pp. 63–114.

Briqueu L., Bougault H. & Joron J.L. 1984. Quantification of Nb, Ta, Ti and V anomalies in magmas associated with subduction zones: petrogenetic implications. *Earth Planet. Sci. Lett.* 68, 297–308.

Buchs D.M., Bagheri S., Martin L., Hermann J. & Arculus R. 2013: Paleozoic to Triassic ocean opening and closure preserved in Central Iran: Constraints from the geochemistry of meta-igneous rocks of the Anarak area. *Lithos* 172–173, 267–287.

Cathelineau M. 1988: Cation site occupancy in chlorites and illites as a function of temperature. *Clay Miner.* 23, 471–485.

Condie K.C., 2001. Mantle Plumes and Their Record in earth History. *Cambridge University Press*, Oxford, UK.

Condie K.C. 2005: High field strength element ratios in Archean basalts: a window to evolving sources of mantle plumes? *Lithos* 79, 491–504.

Dachs E. 2004: PET: Petrological Elementary Tools for Mathematica (R): an update. *Computers & Geosciences* 30, 173–182.

De Paolo D.J. 1981: Trace element and isotopic effects of combined wallrock assimilation and fractional crystallization. *Earth and Planetary Science Letters* 53, 189–202.

Deevsalar R., Ghorbani M.R., Ghaderi M., Ahmadian J., Murata M., Ozawa H. & Shinjo R. 2014: Geochemistry and petrogenesis of arc-related to intraplate mafic magmatism from the Malayaer-Boroujerd plutonic complex, northern Sanandaj-Sirjan magmatic zone, Iran. *Neues Jahrb. Geol. Paläontol. Abh.* 274, 1, 81–120.

Deng H., Kusky T., Polat A., Wang L., Wang J. & Wang S. 2013: Geochemistry of Neoarchean mafic volcanic rocks and late mafic dikys in the Zanhung Complex, Central Orogenic Belt, North China Craton: Implications for geodynamic setting. *Lithos* 175–176, 193–212.

Ernst R.E. & Buchan K.L. 2001: Large mafic magmatic events through time and links to mantle plume heads. In: Ernst R.E. & Buchan K.L. (Eds.): Mantle plumes: their identification through time. *Geol. Soc. Amer., Spec. Pap.* 352, 483–575.

Ernst R.E. & Buchan K.L. 2002: Maximum size and distributions in time and space of mantle plumes: evidence from large igneous provinces. *J. Geodynamics* 34, 309 – 342.

Fergusson C.L., Nutman A.P., Mohajjel M. & Bennett V. 2016: The Sanandaj–Sirjan Zone in the Neo-Tethyan suture, western Iran: Zircon U–Pb evidence of late Palaeozoic rifting of northern Gondwana and mid-Jurassic orogenesis. *Gondwana Res.* 40, 43–57.

Fitton J.G., Saunders A.D., Norry M.J., Hardarson B.S. & Taylor R.N. 1997: Thermal and chemical structure of the Iceland plume. *Earth Planet. Sci. Lett.* 153, 197–208.

Frizon de Lamotte D., Tavakoli-Shirazi S., Leturmy P., Averbuch O., Mouchot N., Raulin C., Lepartmentier F., Blanpied C. & Ringenbach J.C. 2013: Evidence for Late Devonian vertical movements and extensional deformation in northern Africa and Arabia: integration in the geodynamics of the Devonian world. *Tectonics* 32, 1–16.

Ghasemi H., Juteau T., Bellon H., Sabzehei M., Whitechurch H. & Ricou L.E. 2002: The mafic-ultramafic complex of Sikhoran (Central Iran): a polygenetic ophiolite complex. *C.R. Geosci.* 334, 431–438.

Ghazi A.M., Hassanipak A.A., Tucker P.J., Mobasher K. & Duncan R.A. 2001: Geochemistry and ^{40}Ar–^{39}Ar ages of the Mashhad ophiolite, NE Iran: a rare occurrence of a 300 Ma (Paleo-Tethys) oceanic crust. *American Geophysical Union, Fall Meeting 2001*, Abstract I/12C-0993.

Goldberg A.S. 2010: Dyke swarms as indicators of major extensional events in the 1.9–1.2 Ga Columbia supercontinent. *J. Geodynamics* 50, 176–190.

Goodfellow W.D., Cecile M.P. & Leybourne M.I. 1995: Geochemistry, petrogenesis and tectonic setting of lower Paleozoic alkalic and potassic volcanic rocks, Northern Canadian Cordilleran Miogeocline. *Can. J. Earth Sci.* 32, 1236–1254.

Haase K.M. & Devey C.W. 1994: The petrology and geochemistry of Vesteris Seamount, Greenland Basin-an intraplate alkaline volcano of non-plume origin. *J. Petrology* 35, 295–328.

Hafkenscheid E., Wortel M.J.R. & Spakman W. 2006: Subduction history of the Tethyan region derived from seismic tomography and tectonic reconstructions. *J. Geophys. Res.* 111, B08401.

Halls H.C. & Fahrig W.F. 1987: Mafic dyke swarms. *Geol. Assoc. Canada Spec. Pap.* 34, 1-502.

Hammarstrom J.M. & Zen E.A. 1986: Aluminium in hornblende: an empirical igneous geobarometer. *Am. Mineral.* 71, 1297–1313.

Handler R., Neubauer F., Velichkova S.H. & Ivanov Z. 2004: $^{40}Ar/^{39}Ar$ age constraints on the timing of magmatism and post-magmatic cooling in the Panagyurishte region, Bulgaria. *Schweiz. Mineral. Petrogr. Mitt.* 84, 119–132.

Hassanzadeh J. & Wernicke B.P. 2016: The Neotethyan Sanandaj-Sirjan zone of Iran as an archetype for passive margin-arc transitions. *Tectonics* 35, 586-621.

Hochstedter A.G., Gill J.B. & Morris J.D. 1990: Volcanism in the Sumisu Rift, II. Subduction and non-subduction related components. *Earth Planet. Sci. Lett.* 100, 195–209.

Holland T. & Blundy J. 1994: Nonideal interactions in calcic amphiboles and their bearing on amphibole-plagioclase thermometry. *Contrib. Mineral. Petrol.* 116, 433–447.

Hollister L.S., Grissom G.C., Peters E.K., Stowell H.H. & Sisson V.B. 1987: Confirmation of the empirical correlation of Al in hornblende with pressure of solidification of calc-alkaline plutons. *Am. Mineral.* 72, 231–239.

Honarmand M., Li X.H., Nabatian G. & Neubauer F. 2017: In-situ zircon U-Pb age and Hf-O isotopic constraints on the origin of the Hasan-Robat A-type granite from Sanandaj–Sirjan zone, Iran: implications for reworking of Cadomian arc igneous rocks. *Mineral. Petrol.*, doi:10.1007/s00710-016-0490-y.

Jiang Y.H., Ling H.F., Jiang S.Y., Fan H.H., Shen W.Z. & Ni P. 2005: Petrogenesis of a Late Jurassic Peraluminous Volcanic Complex and its High-Mg, Potassic, Quenched Enclaves at Xiangshan, Southeast China. *J. Petrology* 46, 1121–1154.

Kargaranbafghi F., Neubauer F. & Genser J. 2015: The tectonic evolution of western Central Iran seen through detrital white mica. *Tectonophysics* 651–652, 138–151.

Kaygusuz A., Arslan M., Siebel W., Sipahi F. & Ilbeyli N. 2012: Geochronological evidence and tectonic significance of Carboniferous magmatism in the southwest Trabzon area, eastern Pontides, Turkey. *Int. Geol. Rev.* 54, 15, 1776–1800.

Khanna T.C., Sai V.V.S., Zhao G.C., Rao D.V.S., Krishna A.K., Sawant S.S. & Charan S.N. 2013: Petrogenesis of mafic alkaline dikes from the ~2.18 Ga Mahbubnagar Large Igneous Province, Eastern Dharwar Craton, India: Geochemical evidence for uncontaminated intracontinental mantle derived magmatism. *Lithos* 179, 84–98.

Kohn B.P., Eyal M. & Feinstein S. 1992: A major Late Devonian–Early Carboniferous (Hercynian) thermotectonic event at the NW margin of the Arabian-Nubian Shield: Evidence from zircon fission track dating. *Tectonics* 11, 1018–1027.

Khudoley A.K., Prokopiev A.V., Chamberlain K.R., Ernst R.E., Jowitt S.M., Malyshev S.V., Zaitsev A.I., Kropachev A.P. & Koroleva O.V. 2013: Early Paleozoic mafic magmatic events on the eastern margin of the Siberian craton. *Lithos* 174, 44–56.

Leake B. E., Woolley A.R., Arps C.E.S., Birch W.D., Gillbert M.C., Grice J.D., Hawthorne F.C., Kato A., Kirsh H.J., Krivovichev V.G., Linthout K., Laird J., Mandarino J., Maresch W.V., Nichel E.H., Rock N.M.S., Schumacher J.C., Smith D.C., Stephenson N.C.N., Ungaretti L., Whittaker E.J.W. & Youzhi G. 1997: Nomenclature of amphiboles: report of the subcommittee on amphiboles of the International Mineralogical Association Commission on New Minerals and Minerals Names. *Mineral. Mag.* 61, 295–321.

Leitch A.M. & Davies G.F. 2001: Mantle plumes and flood basalts: Enhanced melting from plume ascent and an eclogite component. *J. Geophys. Res.* 106, 2047–2059.

Li B., Bagas L., Gallardo L.A., Said N., Diwu C.H. & McCuaig T.C. 2013: Back-arc and post-collisional volcanism in the Paleoproterozoic Granites-Tanami Orogen, Australia. *Precambrian Res.* 224, 570–587.

Lin P.N., Stem R.J., Morris J. & Bloomer S.H. 1990: Nd- and Sr-isotopic compositions of lavas from the northern Mariana and southern Volcano arcs: implications for the origin of island arc melts. *Contrib. Mineral. Petrol.* 105, 381–392.

Ludwig K.R. 2003: ISOPLOT 3: a geochronological toolkit for Microsoft Excel. *Berkeley Geochronology Centre*, *Spec. Publ.* 4, 1–72.

Maurice CH., David J., O'Neil J. & Francis D., 2009: Age and tectonic implications of Paleoproterozoic mafic dyke swarms for the origin of 2.2 Ga enriched lithosphere beneath the Ungava Peninsula, Canada. *Precambrian Res.* 174, 163–180.

McDonough W.F. & Sun S.S. 1995: The composition of the Earth. *Chem. Geol.* 120, 223–254.

McDougall I. & Harrison M.T. 1999: Geochronology and Thermochronology by the $^{40}Ar/^{39}Ar$ Method. *University Press*, Oxford, 1–269.

Moghadam H.S., Li X. H., Ling X.X., Stern R.J., Santos J.F., Meinhold G., Ghorbani G. & Shahabi S. 2015: Petrogenesis and tectonic implications of Late Carboniferous A-type granites and gabbronorites in NW Iran: Geochronological and geochemical constraints. *Lithos* 212–215, 266–279.

Mohajjel M. & Fergusson C. 2000: Dextral transpression in Late Cretaceous continental collision Sanandaj–Sirjan zone western Iran. *J. Struct. Geol.* 22, 1125–1139.

Morimoto N. 1988: Nomenclature of pyroxenes. *Mineral. Petrol.* 39, 55–76.

Nutman A.P., Mohajjel M., Bennett V.C. & Fergusson C.L. 2014. Gondwanan Eoarchean–Neoproterozoic ancient crustal material in Iran and Turkey: zircon U–Pb–Hf isotopic evidence. *Can. J. Earth Sci.* 51, 272–285.

Ordóñez-Calderón J.C., Polat A., Fryer B.J. & Gagnon J.E. 2011: Field and geochemical characteristics of Mesoarchean to neoarchean volcanic rocks in the Storø greenstone belt, SW Greenland: Evidence for accretion of intra-oceanic volcanic arcs. *Precambrian Res.* 184, 24–42.

Pearce J.A. 2008: Geochemical fingerprinting of oceanic basalts with applications to ophiolite classification and the search for Archean oceanic crust. *Lithos* 100, 14–48.

Peng P., Bleeker W., Ernst E.R., Söderlund U. & McNicoll V. 2011: U–Pb baddeleyite ages, distribution and geochemistry of 925 Ma mafic dykes and 900 Ma sills in the North China craton: Evidence for a Neoproterozoic mantle plume. *Lithos* 127, 210–221.

Pirajno F. & Hoatson D.M. 2012: A review of Australia's Large Igneous Provinces and associated mineral systems: Implications for mantle dynamics through geological time. *Ore Geol. Rev.* 48, 2–54.

Renne P.R., Mundil R., Balco G., Min K. & Ludwig K.R. 2010: Joint determination of ^{40}K decay constants and $^{40}Ar^{*}/^{40}K$ for the Fish Canyon sanidine standard, and improved accuracy for $^{40}Ar/^{39}Ar$ geochronology. *Geochim. Cosmochim. Acta* 74, 18, 5349–5367.

Rieser A.B., Liu Y., Genser J., Neubauer F., Handler R., Friedl G. & Ge X.H. 2006: $^{40}Ar/^{39}Ar$ ages of detrital white mica constrain the Cenozoic development of the intracontinental Qaidam Basin, China. *Geol. Soc. Am. Bull.* 118, 1522–1534.

Scaillet S. 2000: Numerical error analysis in $^{40}Ar/^{39}Ar$ dating. *Earth Planet. Sci. Lett.* 162, 269–298.

Saccani E., Azimzadeh Z., Dilek Y. & Jahangiri A. 2013: Geochronology and petrology of the Early Carboniferous Misho Mafic Complex (NW Iran), and implications for the melt evolution of Paleo-Tethyan rifting in Western Cimmeria. *Lithos* 162, 264–278.

Shakerardakani F., Neubauer F., Masoudi F., Mehrabi B., Liu X., Dong Y., Mohajjel M., Monfaredi B. & Friedl G., 2015. Panafrican basement and Mesozoic gabbro in the Zagros orogenic belt in the Dorud-Azna region (NW Iran): Laser-ablation ICP-MS zircon ages and geochemistry. *Tectonophysics* 647–648, 146–171.

Shakerardakani F., Neubauer F., Bernroider M., Finger F., Genser J., Waitzinger M. & Monfaredi B. (submitted). Conditions and timing of metamorphism in the central Sanandaj-Sirjan zone (Zagros Mountains, Iran): A case of polymetamorphism. *J. Metamorph. Geol.*

Sharifi M. & Sayari M. 2013: Alkaline basic dykes in the central part of Sanandaj-Sirjan zone (Iran). *J. Tethys* 1, 41–58.

Sheikholeslami R., Bellon H., Emami H., Sabzehei M. & Pique A. 2003: Nouvelles données structurales et datations $^{40}K/^{40}Ar$ surles roches métamorphiques de la région de Neyriz (zone de Sanandaj-Sirjan, Iran méridional). Leur intérêt dans le carde du domaine néo-téthysien du Moyen-Orient. *C.R. Geosci.* 335, 981–991.

Shervais J.W. 1982: Ti–V plots and the petrogenesis of modern and ophiolitic lavas. *Earth .Planet. Sci. Lett.* 59, 101–118.

Shinjo R., Chung S.L., Kato Y. & Kimura M. 1999: Geochemical and Sr-Nd isotopic characteristics of volcanic rocks from the Okinawa Trough and Ryukyu Arc: Implications for the evolution of a young, intracontinental back arc basin. *J. Geophys. Res.* 104, 591–608.

Srivastava R.K. 2011: Dyke Swarms: Keys for Geodynamic Interpretation. *Springer*, Heidelberg, 1–603.

Stern R.J., Ren M., Ali K., Förster H.J., Al Safarjalani A., Nasir S., Whitehouse M.J., Leybourne M.I. & Romer R.L. 2014: Early Carboniferous (~357 Ma) crust beneath northern Arabia: Tales from Tell Thannoun (southern Syria). *Earth Planet. Sci. Lett.* 393, 83–93.

Sun S.S. & McDonough W.F. 1989: Chemical and isotopic systematic of ocean basalts: implication for mantle composition and processes. In: Saunders, A.D., Norry, M.J. (Eds.), Magmatism in the ocean basins. *Geol. Soc. London, Spec. Publ.* 42, 313–345.

Tavakoli-Shirazi S., Frizon de Lamotte D., Wrobel-Daveau J-C. & Ringenbach J.C. 2013: Pre-Permian uplift and diffuse extensional deformation in the High Zagros Belt (Iran): integration in the geodynamic evolution of the Arabian plate. *Arab. J. Geosci.* 6, 2329–2342.

Taylor S.R. & McLennan S.M. 1985: The Continental Crust: Its Composition and Evolution: an Examination of the geochemical record preserved in Sedimentary Rocks. *Blackwell Scientific*, Oxford, i–xv, 1–312.

Topuz G., Altherr R., Siebel W., Schwarz W.H., Zack T., Hasözbek A., Barth M., Satır M. & Şen C. 2010: Carboniferous high-potassium I-type granitoid magmatism in the eastern Pontides: The Gümüşhane pluton (NE Turkey). *Lithos* 116, 92–110.

Van Staal C.R., Winchester J.A. & Bédard J.H. 1991: Geochemical variations in Middle Ordovician volcanic rocks of the northern Miramichi Highlands and their tectonic significance. *Can. J. Earth Sci.* 28, 1031–1049.

Von Quadt A., Gunther D., Frischknecht R. & Dietrich V. 1999: Minor and trace element determinations in Li2B407 fused USGS standard materials calibrated without matrix-matched standards using laser ablation ICP-MS. *J. Conference Abstracts* 4, 819.

Wang K., Plank T., Walker J.D. & Smith E.I. 2002: A mantle melting profile across the Basin and Range, SW USA. *J. Geophys. Res.* 107, B1, 2017, http://dx.doi.org/10.1029/2001JB000209.

Winchester J.A. & Floyd P.A. 1977: Geochemical discrimination of different magma series and their differentiation products using immobile elements. *Chem. Geol.* 20, 325–343.

Wood D.A. 1980: The application of a Th-Hf-Ta diagram to problems of tectonomagmatic classification and to establishing the nature of crustal contamination of basaltic lavas of the British Tertiary Volcanic Province. *Earth Planet. Sci. Lett.* 50, 11–30.

Zanchetta S., Zanchi A., Villa I.M., Poli S. & Muttoni G. 2009: The Shanderman eclogites: a Late Carboniferous high-pressure event in the NW Talesh Mountains (NW Iran). *Geol. Soc. London, Spec. Publ.* 312, 57–78.

Zanchetta S., Berra F., Zanchi A., Bergomi M., Caridroit M., Nicora A. & Heidarzadeh G. 2013: The record of the Late Palaeozoic active margin of the Palaeotethys in NE Iran: constraints on the Cimmerian orogeny. *Gondwana Res.* 24, 1237–1266.

Zanchi A., Zanchetta S., Berra F., Mattei M., Garzanti E., Molyneux S., Nawab A. & Sabouri J. 2009a: The Eo□Cimmerian (Late? Triassic) orogeny in North Iran. *Geol. Soc. London, Spec. Publ.* 312, 31–55.

Zanchi A., Zanchetta S., Garzanti E., Balini M., Berra F., Mattei M. & Muttoni G. 2009b: The Cimmerian evolution of the Nakhlak–Anarak area, central Iran, and its bearing for the reconstruction of the history of the Eurasian margin. *Geol. Soc. London, Spec. Publ.* 312, 261–286.

Zhang, C.L., Zou, H.B., Yao, C.Y. & Dong, Y.G. 2014: Origin of Permain gabbroic intrusions in the southern margin of the Altai Orogenic belt: A possible link to the Permian Tarim mantle plume? *Lithos* 204, 112–124.